



Sushil Bacha, B.E in Automation and Robotics

Robust control of Wind turbine systems

Master's Thesis

Master of Science

Control and Robotics(CORO): Control Systems(CSYS)

submitted to

Ecole Centrale de Nantes

Supervisor

Prof. Franck Plestan
Elias Tahoumi, PhD candidate at ECN

Nantes, August 2019

Contents

1	Introduction	3
2	Modelling of the SEREO structure	4
2.1	Aerodynamic and mechanical model	5
2.2	Blade pitch dynamics	6
2.3	Yaw dynamics	7
2.4	Electrical model	7
3	Nonlinear model of SEREO system	8
4	Control problem statement	9
5	Control strategy	10
5.1	Some recalls	11
5.2	Control design	12
6	Adaptive FOSMC of TWT	13
6.1	Results	16
7	Differentiator	21
7.1	Results	22
8	Adaptive HOSMC of TWT	26
8.1	Results	28
8.2	Noisy scenario	33
8.2.1	FOSMC vs HOSMC(adaptive and non-adaptive)	34
9	Wind direction	38
10	Future works	39
10.1	Results	41
11	Conclusion	46

Abstract

This thesis focuses on proposing new schemes for wind turbine systems. Among the studied systems, there is SEREO concept that is a twin wind turbine (TWT) [1] system. This system includes two identical wind turbines ridden on the same tower, which can pivot face the wind with no additional actuator (see Fig.1). The controller scheme allows forcing the system to face the wind, to produce the maximal power and to limit the structural vibrations by acting on the electromagnetic torques.



Figure 1: SEREO structure [1]

Robust controllers have previously been designed for this system by supposing similar wind conditions for both wind turbines [5]. The control law implemented in this thesis is based on Sliding Mode Control (SMC). It is well known that sliding mode controllers are robust against perturbations but consume a large amount of energy. An adaptive second-order sliding mode controller is implemented which reduces the energy consumption while keeping robustness. This controller is efficient for systems with uncertainties and external perturbations and is compared with first-order sliding mode control. This new controller will be evaluated with respect to performances indicators.

This controller is also based on a state pre-feedback that requires informations derived by time differentiation of measured variables. A very recent novel differentiation [9] solution is used to provide information to the controller. This differentiation scheme allows to achieve high accuracy, to reduce the noise effect and then to get a noise-reduced controller.

1 Introduction

The original feature of SEREO versus standard turbines is due to the fact that the rotation of the arms carrying the two wind turbines is free: indeed, no additional yaw driving motor is required to track the wind direction. The advantages of such structure are

- given that there is no yaw actuation, failures risks are reduced, as well as maintenance;
- furthermore, on a same tower, two turbines are available. Efficiency of power generated is high when compared to standard turbines.

However, as previously mentioned, it is necessary to design an appropriate control strategy to align the turbines face the wind. Concerning the electrical part of the system, the two wind turbines are associated with two permanent magnet synchronous generators(PMSG). (see Table 1)

Mechanical parameters		Parameters of PMSG	
Blade radius R	39 m	Rated power	2 MW
Air density ρ	1.205 kg/m ³	Stator resistance R_s	50 $\mu\Omega$
Rated wind speed	12 m/s	d axis inductance L_d	0.0055 H
Maximum power coefficient	0.4	q axis inductance L_q	0.00375 H
Total inertia J	10,000 kg m ²	Pole pairs number p	11
Yaw inertia K_r	5 . 10 ⁵ kg m ²	Field flux Φ_f	136.25 Wb
Yaw friction coefficient D_r	200 N m/(rad/s)		
Length L	40 m		

Table 1: Parameters of the wind turbines

In order to reach a high efficiency, two objectives have to be managed: the first one consists in controlling the position of the wind turbine with respect to the wind direction whereas the second controller is devoted to the electrical generator. The rotor speed of the wind turbine is controlled by maintaining the tip speed ratio at its optimum value [2],[3],[4]. In fact, the wind turbine is the most efficient if it is face the wind. In the framework of the power maximization by following the wind direction, it is worth mentioning [6], where the MPPT (Maximum Power Point Tracking) technique is combined with the active yaw control.

Due to this fact with SEREO, no additional yaw actuator is required to follow the wind direction; It is shown via simulations that the designed control scheme successfully forces the structure to face the wind while keeping optimal energy production. Two aspects of the control are considered

- mechanical: controlling the yaw motion of the structure in order to orient it face the wind by acting on the blade pitch angle of both twin turbines.
- electrical: forcing the direct current of both generators to 0 to limit the ripple effect on the electromagnetic torque and controlling the angular velocities of both generators in order to optimize the electrical power output. This is achieved by acting on the direct and quadrature stator voltages.

In [5], it has been shown that this structure can be oriented by controlling the pitch blades angles of the two wind turbines, hence creating a difference between the drag forces of the two rotors. Another strategy has been proposed in [7], in which the difference of drag forces is produced by acting on the generator torques, Given that the system is controlled in a very perturbed environment, a robust controller is required to deal with uncertainties and external disturbances. In [5], the first order sliding mode (SM) based controller has shown its efficiency in terms of accuracy for wind direction tracking and power optimization, over a PI-based controller. However, the evaluation of the drive train oscillations has revealed that it would be important to reduce these phenomena, to mitigate fatigue loads of the structure (a key-point in wind turbines control). Then, in [7] a controller based on the super-twisting (ST) algorithm [8], acting on the electro-magnetic torques to force the rotation of the structure facing the wind has been presented. A comparison with standard SM controller has shown the improvements of

this approach regarding reduction of drive train oscillations. Here, in this project, a difference between the drag forces of the turbines is created by varying the pitch angle of the two wind turbines.

The SEREO system including mechanical and electrical parts, is a nonlinear system where it is greatly disturbed (wind variations, parametric uncertainties, ..) Furthermore, the variable speed-variable pitch wind turbines are expected to operate in large scale of the wind velocity. Due to these features, it is crucial to develop control laws which are robust with respect to uncertainties and perturbation, and which are efficient over a large operating domain.

Parametric uncertainties of PMSG	
Resistance(R)	20%
Inductance (L_d)	20%

During the thesis, an adaptive sliding mode controller [30],[31],[32],[33],[34] has been implemented. This approach is known to be robust versus parametric uncertainties and perturbations and quite easy to tune.

The main contributions are

- Control of the both mechanical and electrical parts of SEREO structure, based on sliding mode approach,
- Evaluation of the closed-loop system performances under different scenarios (structure face the wind, structure not face the wind, parametric uncertainties, ..)
- Performances comparison (standard deviation of the electromagnetic torques and the mean power) of the SMC versus Adaptive sliding mode control.

Sliding mode control (SMC) [11],[12],[42] is a very well known robust control method for uncertain nonlinear systems. It is mainly recognized for its robustness against perturbations/uncertainties and high accuracy where these features make it ideal for many applications. However, the main drawback of the standard is the chattering phenomenon *i.e.* high frequency oscillations which may damage physical components such as actuators and decrease the accuracy with respect to a sampled controller. It is also restricted to systems with input-output relative degree equal to 1 . Higher order sliding mode (HOSM)[43],[44],[45] techniques have been designed to deal with these drawbacks.

Adaptive HOSMC is based on linear and twisting controllers: a time-varying parameter allows the controller to balance between a linear controller and the twisting one [30],[31],[32],[33],[34]. The obtained controller has the advantages of the twisting controller [8] (accuracy and robustness) and of the second order linear state feedback (low energy consumption). The twisting controller known for its high accuracy and robustness with respect to matching perturbations/uncertainties. However, the gains are overestimated resulting in a high energy consuming controller from a control effort point of view. Controller has the advantages of the homogeneous one in (accuracy and robustness), but with its drawbacks (chattering and high energy consumption) strongly reduced. This is made possible by introducing a parameter on the exponent term of the homogeneous controller, this parameter varying between 0 and 1 and depending on the accuracy of the tracking.

2 Modelling of the SEREO structure

In this section, a full model of the SEREO structure is detailed and composed of the aerodynamic model, pitch angle dynamics, yaw dynamics, and angular velocities/direct-quadratic currents dynamics of the generators.

2.1 Aerodynamic and mechanical model

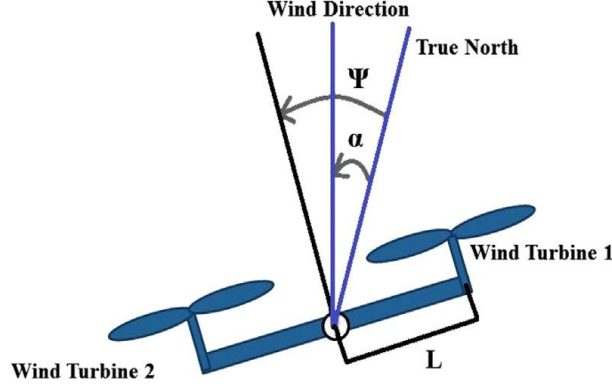


Figure 2: Simplified representation of the twin wind turbines (view from the top)

Fig.2 displays a scheme of the SEREO structure, viewed from the top. One supposes that the two turbines have the same features. In the rest of the paper, the twin turbines are denoted with an index i , such that $i \in \{1, 2\}$, which gives Turbine 1 and Turbine 2. From Fig.2, α (resp. ψ) is the angle between the True North and the wind direction (resp. the orientation of the wind turbines defined by an axis that is perpendicular to the arm connecting the two turbines). The mechanical power P_{ai} captured by each turbine from the wind, the aerodynamic torque Γ_{ai} and the drag force F_{di} are given by ($i \in \{1, 2\}$) [13]

$$P_{ai} = \frac{1}{2} C_{p,i}(\lambda_i, \beta_i) \rho \pi R^2 (V \cos(\psi - \alpha))^3 \quad (1)$$

$$\tau_{ai} = \frac{1}{2} \frac{C_{p,i}(\lambda_i, \beta_i)}{\lambda_i} \rho \pi R^3 (V \cos(\psi - \alpha))^2 \quad (2)$$

$$F_{di} = \frac{1}{2} C_{d,i}(\lambda_i, \beta_i) \rho \pi R^2 (V \cos(\psi - \alpha))^2 \quad (3)$$

with R the radius of the wind turbines blades, ρ the air density, V the wind velocity, β_i the pitch angle of the blades, and λ_i the tip-speed ratio (TSR) which is defined as

$$\lambda_i = \frac{\Omega_i}{V \cos(\psi - \alpha)} R. \quad (4)$$

The power coefficient $C_{p,i}$ depends on the TSR and the pitch angle [3],[14] and reads as

$$C_{p,i}(\lambda_i, \beta_i) = c_1(c_2 a - c_3 \beta_i - c_4) e^{-c_5 a} \quad (5)$$

with

$$a = \frac{1}{\lambda_i + 0.08\beta_i} - \frac{0.035}{\beta_i^3 + 1}$$

and

$$c_1 = 0.22 \quad c_2 = 116 \quad c_3 = 0.4 \quad c_4 = 12.5 \quad c_5 = 21.$$

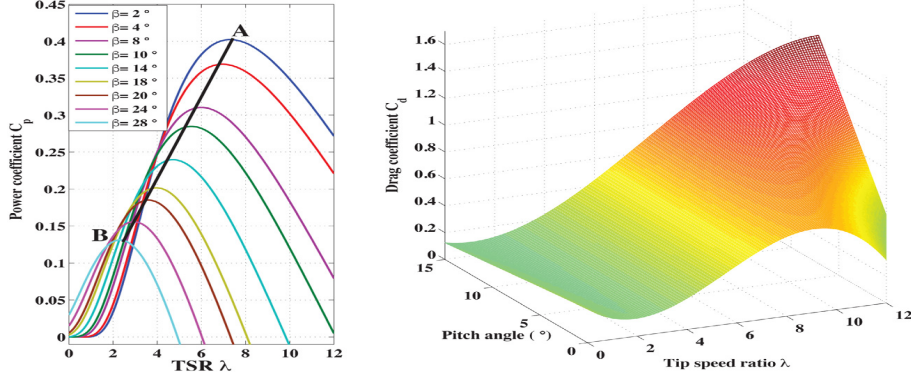


Figure 3: Left(a)-Power coefficient C_p versus the tip-speed ratio λ , for different values of pitch angle. Right(b)-drag coefficient C_d versus the tip-speed ratio λ and the pitch angle β .

Fig. 3 displays the evolution of the power coefficient versus the TSR, for different values of the pitch angle of the blades. As detailed in the control section, the objective consists in producing the maximal electrical power: it means that the system must be controlled to get a maximal value of $C_{p,i}$. It means also that the pitch angle, β_i and the TSR, λ_i have to be adjusted to reach this objective. The black bold curve (AB) (Fig. 3) corresponds to the optimal power coefficient. Along this curve, by applying the MPPT (Maximum Point Power Tracking) strategy [15], the wind turbine operates in high efficiency to produce the maximal energy. Finally, this optimal curve allows to link the tip-speed ratio λ_i and an optimal pitch angle β_i^{opt} , which corresponds to an optimal value of power coefficient $C_{p,i}^{\text{opt}}$ [16],[46] the link is given by the following function

$$\beta_i^{\text{opt}} = 0.0219\lambda_i^4 - 0.2810\lambda_i^3 + 0.4421\lambda_i^2 + 11.8415\lambda_i - 7.9378 \quad (6)$$

The drag coefficient $C_{d,i}$ [18] is a nonlinear function of the TSR and the pitch angle. From [18], a least squares polynomial interpolation method allows to get an expression of $C_{d,i}$ that reads as

$$C_{d,i}(\lambda_i, \beta_i) = \underbrace{a_0 + a_1\lambda_i + a_2\lambda_i^2 + a_3\lambda_i^3}_{A_i} + \underbrace{(b_0 + b_1\lambda_i + b_2\lambda_i^2 + b_3\lambda_i^3)}_{B_i} \cdot \beta_i \quad (7)$$

with

$$a_0 = 0.25382, a_1 = -0.1369, a_2 = 0.04345, a_3 = -0.00263,$$

$$b_0 = -0.008608, b_1 = 0.0063, b_2 = -0.0015, b_3 = 0.000118$$

2.2 Blade pitch dynamics

As mentioned previously, the blade pitch angles β_1 and β_2 can be modified, in order to modify the drag forces F_{d1} and F_{d2} allowing to force the rotation of the SEREO structure. The dynamics of the pitch angles actuators of the two wind turbines can be written as a first order system [17],[19],

$$\dot{\beta}_1 = \frac{1}{T_{\beta_1}}\beta_1^* - \frac{1}{T_{\beta_1}}\beta_1 \quad (8)$$

$$\dot{\beta}_2 = \frac{1}{T_{\beta_2}}\beta_2^* - \frac{1}{T_{\beta_2}}\beta_2$$

with $T_{\beta_1} = T_{\beta_2}$ being the time constants of the blades actuation system and β_1^*, β_2^* the pitch angles references. The formulation of the model (8) supposes that there is an inner loop for the control of both pitch angles: the static gain equals 1, *i.e.* the positioning is ideal, only the response time is taken into account through the time

constants T_{β_1}, T_{β_2} . Of course, all the challenge consists in determining the values of β_1^* and β_2^* in order to ensure an optimal behavior of the system. The control strategy will be detailed in the sequel; however, some elements are given here to introduce definitions of β_1^* and β_2^* .

Definition of pitch angles references β_1^* and β_2^* . The wind turbines have to be face the wind to produce maximal energy: in this case, the control strategy will force the both ones to have the same angular velocities (in magnitude) in order to stabilize the structure face the wind.

However, by a practical point-of-view, it is not possible to have Ω_1 and Ω_2 with strictly the same magnitude. From (6), one gets, for the both wind turbines, the optimal values of the pitch angles denoted β_1^{opt} and β_2^{opt} . In this case, i.e., if the structure is face the wind, one has

$$\beta_1^* = \beta_1^{opt}$$

$$\beta_2^* = \beta_2^{opt}$$

If the wind direction is changing, it is necessary to generate a difference between the drag forces F_{d1} and F_{d2} , by acting on the pitch angles and their references. Then, the pitch angles references β_1^* and β_2^* become

$$\beta_1^* = \beta_1^{opt} + \Delta\beta_1$$

$$\beta_2^* = \beta_2^{opt} + \Delta\beta_2$$

with $\beta_1^{opt}, \beta_2^{opt}$ defined from (6) and $\Delta\beta_1$ and $\Delta\beta_2$ being viewed as the control inputs controlling the rotation of the structure.

2.3 Yaw dynamics

The dynamics of the rotation of the SEREO structure around its vertical axis is given by

$$K_r \ddot{\psi} = -D_r \dot{\psi} + (F_{d1} - F_{d2}) L$$

with K_r and D_r the inertia moment and the friction coefficient, respectively, associated to yaw motion, and L the length between the horizontal axis and the vertical axis (Fig. 2). From (1) – (7), one gets

$$\begin{aligned} F_{d1} - F_{d2} &= \frac{1}{2} \rho \pi (RV \cos(\psi - \alpha))^2 (C_{d,1} - C_{d,2}) \\ &= \frac{1}{2} \rho \pi (RV \cos(\psi - \alpha))^2 [\mathcal{A}_1 - \mathcal{A}_2 + \mathcal{B}_1 \cdot \beta_1 - \mathcal{B}_2 \cdot \beta_2] \end{aligned}$$

2.4 Electrical model

The Permanent Magnet Synchronous Generator is widely used for the industrial applications (automobiles, conversion energy system), thanks to their high efficiency and large torque current ratio [20]. Its standard mathematical model, in the synchronous reference frame (d, q) is given by [21] and [22]

$$\begin{aligned} \dot{i}_{di} &= \frac{-R_s}{L_d} i_{di} + \frac{pL_q}{L_d} \Omega i_{qi} + \frac{1}{L_d} V_{di} \\ \dot{i}_{qi} &= \frac{-R_s}{L_q} i_{qi} - \frac{pL_d}{L_q} \Omega_{di} - \frac{p\phi_f}{L_q} \Omega_i + \frac{1}{L_q} V_{qi} \\ \dot{\Omega}_i &= \frac{1}{J} \Gamma_{ai} - \frac{p[(L_d - L_q) i_{di} + \phi_f]}{J} i_{qi} - \frac{f_v}{J} \Omega_i \end{aligned}$$

where $i_{di}, i_{qi}, V_{di}, V_{qi}$ are respectively the stator currents and stator voltages, L_d, L_q are the dq -axis inductances, R_s is the stator resistance, p is the number of pole pairs, ϕ_f permanent-magnet flux linkage, J is the total inertia, and f_v the friction coefficient.

3 Nonlinear model of SEREO system

The SEREO system can be written as a nonlinear system affine with respect to the control input vector

$$\dot{x} = f(x) + g(x) \cdot u \quad (9)$$

with x the state vector and u the input vector respectively defined as

$$x = [\beta_1 \quad \beta_2 \quad \psi \quad \dot{\psi} \quad i_{d1} \quad i_{q1} \quad \Omega_1 \quad i_{d2} \quad i_{q2} \quad \Omega_2]^T \quad (10)$$

$$u = [\beta_1^* \quad \beta_2^* \quad V_{d1} \quad V_{q1} \quad V_{d2} \quad V_{q2}]^T$$

The vector $f(x)$ and the matrix $g(x)$ read as

$$f(x) = \begin{bmatrix} -\frac{1}{T_{\beta_1}}\beta_1 \\ -\frac{1}{T_{\beta_2}}\beta_2 \\ \dot{\psi} \\ \frac{1}{K_r}(-D_r\dot{\psi} + \varphi(\psi, \beta_1, \beta_2, \Omega_1, \Omega_2)L) \\ \frac{-R_s}{L_d}i_{d1} + \frac{pL_q}{L_d}i_{q1}\Omega_1 \\ \frac{-R_s}{L_q}i_{q1} - \frac{pL_d}{L_q}i_{d1}\Omega_1 - \frac{p\phi_f}{L_q}\Omega_1 \\ \frac{1}{J}\Gamma_{a1}(\beta_1, \Omega_1, \psi) - \frac{p\phi_f}{J}i_{q1} - \frac{p(L_d - L_q)}{J}i_{d1}i_{q1} - \frac{f_v}{J}\Omega_1 \\ \frac{-R_s}{L_d}i_{d2} + \frac{pL_q}{L_d}i_{q2}\Omega_2 \\ \frac{-R_s}{L_q}i_{q2} - \frac{pL_d}{L_q}i_{d2}\Omega_2 - \frac{p\phi_f}{L_q}\Omega_2 \\ \frac{1}{J}\Gamma_{a2}(\beta_2, \Omega_2, \psi) - \frac{p\phi_f}{J}i_{q2} - \frac{p(L_d - L_q)}{J}i_{d2}i_{q2} - \frac{f_v}{J}\Omega_2 \end{bmatrix} \quad (11)$$

$$g(x) = \begin{bmatrix} \frac{1}{T_{\beta_1}} & 0 & 0 & 0 & 0 & 0 & 0 & 0 & 0 & 0 \\ 0 & \frac{1}{T_{\beta_2}} & 0 & 0 & 0 & 0 & 0 & 0 & 0 & 0 \\ 0 & 0 & 0 & 0 & \frac{1}{L_d} & 0 & 0 & 0 & 0 & 0 \\ 0 & 0 & 0 & 0 & 0 & \frac{1}{L_q} & 0 & 0 & 0 & 0 \\ 0 & 0 & 0 & 0 & 0 & 0 & 0 & \frac{1}{L_d} & 0 & 0 \\ 0 & 0 & 0 & 0 & 0 & 0 & 0 & 0 & 0 & \frac{1}{L_q} \\ 0 & 0 & 0 & 0 & 0 & 0 & 0 & 0 & 0 & 0 \end{bmatrix} \quad (12)$$

Both angular velocities Ω_1 and Ω_2 have not formally the same magnitude. It gives that $\lambda_1 \neq \lambda_2$, thus $\beta_1^{opt} \neq \beta_2^{opt}$. However, dynamics of angular velocity and pitch angle are different: the motion of the whole structure face the wind is slower than the adaptation of the rotation velocities of wind turbines. Ω_1, Ω_2 are controlled by the electrical inputs control V_{q1} and V_{q2} , respectively. Then, the angular speed tracking is so fast, that it shall not affected by

the pitch angles variation which assumed that are included with the mechanical part. By this way, one states that

Assumption 1. The angular velocities Ω_1 and Ω_2 are the same.

Then, as detailed in the sequel, the both velocities are forced to be equal to a same reference value Ω^* for a given optimum tip speed ratio λ_{opt} . It is concluded that, in the current study, one has

$$\lambda_1 = \lambda_2 = \lambda \quad \text{and} \quad \beta_1^{\text{opt}} = \beta_2^{\text{opt}} = \beta^{\text{opt}}$$

which gives

$$\begin{aligned}\beta_1^* &= \beta^{\text{opt}} + \Delta\beta_1 \\ \beta_2^* &= \beta^{\text{opt}} + \Delta\beta_2\end{aligned}$$

Given that the rotation is made thanks to $F_{d,1}$ and $F_{d,2}$, one states asymmetric behavior, which gives $\Delta\beta_1 = -\Delta\beta_2 = \Delta\beta_2 = \Delta\beta$. Then, one gets

$$\begin{aligned}\beta_1^* &= \beta^{\text{opt}} - \Delta\beta \\ \beta_2^* &= \beta^{\text{opt}} + \Delta\beta\end{aligned}$$

Then, from **Assumption 1**, Eq. (11) reads as

$$\varphi = CB \cdot [\beta_1 - \beta_2]$$

given that $A_1 - A_2 = 0$, and $B_1 = B_2 = B$. Given that the yaw motion is made by acting the pitch angles thanks to the control input $\Delta\beta$, one defines a new control input \bar{u} as

$$\bar{u} = [\Delta\beta \quad V_{d1} \quad V_{q1} \quad V_{d2} \quad V_{q2}]^T \quad (13)$$

The input u is a 6×1 vector whereas \bar{u} is a 5×1 -vector, these both vectors being linearly linked by

$$u = \begin{bmatrix} -1 & 0 & 0 & 0 & 0 \\ 1 & 0 & 0 & 0 & 0 \\ 0 & 1 & 0 & 0 & 0 \\ 0 & 0 & 1 & 0 & 0 \\ 0 & 0 & 0 & 1 & 0 \\ 0 & 0 & 0 & 0 & 1 \end{bmatrix} \cdot \bar{u} + \begin{bmatrix} \beta_{\text{opt}} \\ \beta_{\text{opt}} \\ 0 \\ 0 \\ 0 \\ 0 \end{bmatrix} \quad (14)$$

The input $\Delta\beta$ appears in the time derivative of the pitch angles β_1 and β_2 . From (9) – (14), (21) the relative degree of the yaw angle ψ versus $\Delta\beta$ equals 3.

4 Control problem statement

The control of the SEREO TWT has to ensure optimal production of electrical power. The optimal amount of electrical production depends on the site requirements (power grids, inhabitants, ...); however, one supposes here that the objective is to produce the maximal amount of energy that can produce the both generators (twice 2 MW). In this case, the wind turbines have to be face the wind. In case of a change of wind direction, the rotation of the nacelle [23] is required, in order to maintain the optimal configuration. With SEREO structure, this configuration (optimal energy) is ensured by the combination of the MPPT and the control of the yaw angle rotation. Then, three control problems have to be managed

- Force the structure to be face the wind, *i.e.*, control $\psi - \alpha$ to 0;
- Control the angular velocities of the wind turbines, in order to optimize the electrical power, *i.e.*, control Ω_1 and Ω_2 to an "optimal" reference Ω^* ;

- Control the direct currents of the both generators $i_{d,1}$ and $i_{d,2}$ in order to avoid the ripple effects on the electromagnetic torque [24], i.e., force $i_{d,1}$ and $i_{d,2}$ to 0 .

Note that there is a link between these first objectives: the action on the pitch angles has an influence on the optimal value of λ . A consequence is that, if the structure is not face the wind, the produced energy is not, during the transient time, formally optimal because the pitch angles are not optimal, but used in order to ensure the rotation.

Angular velocities control- As previously explained, the two wind turbines have to reach the maximum power coefficient, by keeping their tip-speed ratios at their optimal values, for given pitch angles of wind turbines blades. Therefore, the rotational speeds of the two wind turbines are controlled at a reference which are derived from λ_{opt} by (4). Then, recalling **Assumption 1**, the reference of the rotational speed reads as

$$\Omega^* = \frac{V \cos(\psi - \alpha)}{R} \lambda_{opt} \quad (15)$$

Direct current control- The ripples of the electromagnetic torque can increase the fatigues loads in the mechanical shaft of the wind turbine, and affect the produced power. In order to avoid these drawbacks, a solution consists in forcing the direct current i_d at zero. The references of the direct currents are given as [24],[25]

$$i_{d,1}^* = i_{d,2}^* = 0 \quad (16)$$

Control of the structure yaw rotation- When the structure is oriented face the wind, there is no difference between the drag forces ($F_{d1} - F_{d2} = 0$) . If the wind direction changes, a yaw error is created (see Fig. 2) ; then, the rotation of the twin wind turbines is required to track the wind direction. The control objective consists in forcing $\psi - \alpha$ to 0. As said above, the rotation of the structure does not require a yaw driven motor. Therefore, the pitch angles of the two wind turbines blades are changed, in order to create a difference between the drag coefficients $C_{d,1}$ and $C_{d,2}$, i.e., between the drag forces F_{d1} and F_{d2} of the both wind turbines. Thanks to this difference, a yawing torque Γ_ψ defined as

$$\Gamma_\psi = (F_{d1} - F_{d2}) L \quad (17)$$

is appearing and forces the motion of the rotation.

Control scheme- The proposed control scheme of the SEREO structure is shown by Fig. 4 .

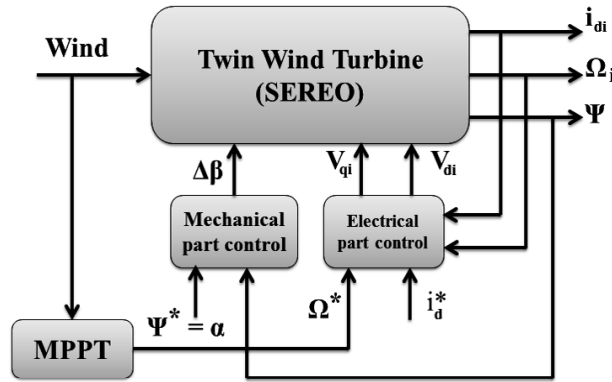


Figure 4: Scheme of the SEREO structure control

5 Control strategy

Several nonlinear control strategies have been used in order to overcome the drawbacks of robustness and limited operating domain. Thus, one can cite **fuzzy-sliding mode control** [39] or **adaptive neural network** [40] which

are quite efficient but are not easy to tune and formally implement. **Switching output feedback controller (SOFc)** [36],[37],[38] keep the use of only the sliding variable(no time derivatives) Based on gain switching at an adequate time. Is applicable to system with relative degree 1 and 2. **Twisting controller (TWC)** [8], requires the information of time derivative of . Previously PI controller was applied [14]. However, the **PI controller** is considered as a linear controller; therefore, an accurate knowledge of the system is required to ensure a good performance [47] and the operating domain of the controller is quite limited. It means that, outside this domain, the control strategy is less efficient in terms of accuracy, disturbance rejection and parametric variations. Gains in the above controllers are overestimated. This can amplify the chattering effect and increase the controller's energy consumption every time.

As detailed in the previous section, the control of the twin wind turbines includes the mechanical part control of the system (yaw control) and the control of its electrical part (direct currents/angular the velocities). In order to design a robust control solution, and given the nonlinear dynamics of the system, the selected control solution is based on **sliding mode control** approach.

The idea of such control strategy is to force the system trajectories to converge to a domain named sliding surface, and to be maintained on it in spite of perturbations and uncertainties, thanks to a discontinuous control input. The main features of this class of control are [26],[27].

- The control input is based on the so-called sliding variable which is determined from the control objectives; from the sliding variable is defined the manifold called sliding surface;
- The control input, which is discontinuous, has to force the system trajectories to reach the sliding surface, in a finite time and in spite of the uncertainties and perturbations;
- Once the sliding surface is reached, the trajectories are evolving on it; the sliding surface is said attractive. By this way, the control objectives are fulfilled in spite of uncertainties and perturbations.

5.1 Some recalls

Consider the nonlinear system

$$\begin{aligned}\dot{z} &= f_z(z) + g_z(z) \cdot \bar{u} \\ y &= h(z, t)\end{aligned}\tag{18}$$

with $z \in \mathcal{Z} \subset R^n$ the state vector, $\bar{u} \in R$ the control input and $y \in R$ the control objective (which means that the control objective consists in forcing y to 0). z is an open subset of R^n . The vector fields $f_z(z)$ and $g_z(z)$ are uncertain. The sliding variable $S(z, t)$ is defined from the control objective y (also called output variable) such that

- $S(z, t) = 0$ induces $y \rightarrow 0$;
- The relative degree of (18) with respect to $S \geq 1$, i.e. $\rho \geq 1$.

Then, from (23), one gets

$$\begin{aligned}\frac{\partial S^{(i)}}{\partial u} &= 0, \quad \forall i < \rho \\ S^{(\rho)} &= \Theta(z, t) + \Lambda(z, t) \cdot \bar{u}\end{aligned}\tag{19}$$

Assumption 2 The functions $\Theta(z, t)$ and $\Lambda(z, t)$ are unknown but bounded, $\forall z \in \mathcal{Z}$ and $t \geq 0$. Furthermore, $\Lambda(\cdot) > 0$.

Assumption 3 The functions $\Theta(\cdot)$ and $\Lambda(\cdot)$ read as

$$\begin{aligned}\Theta(\cdot) &= \Theta_N(\cdot) + \delta\Theta(\cdot) \\ \Lambda(\cdot) &= \Lambda_N(\cdot) + \delta\Lambda(\cdot)\end{aligned}\tag{20}$$

with Θ_N and Λ_N the nominal "well-known" parts, and $\delta\Theta$ and $\delta\Lambda$ the "uncertain" parts, of respectively the

functions Θ and Λ .

Assumption 4 The function Λ_N is such that, $\forall z \in \mathcal{Z}$ and $t \geq 0$, there exist two positive constants Λ_N^m and Λ_N^M such that

$$\begin{aligned} 0 < \Lambda_N^m \leq \Lambda_N \leq \Lambda_N^M, \quad \Lambda_N > 0 \\ 0 < \Lambda_N^m \leq -\Lambda_N \leq \Lambda_N^M, \quad \Lambda_N < 0 \end{aligned}$$

Furthermore, the uncertain term $\delta\Lambda$ is such that, $\forall z \in \mathcal{Z}$ and $t \geq 0$

$$\left| \frac{\delta\Lambda}{\Lambda_N} \right| \ll 1$$

Assumption 5 The function Θ_N is such that, $\forall z \in \mathcal{Z}$ and $t \geq 0$, there exists a positive constant Θ_N^M such that

$$|\theta_N| < \Theta_N^M$$

Furthermore, the uncertain term $\delta\Theta$ is such that, $\forall z \in \mathcal{Z}$ and $t \geq 0$

$$\left| \frac{\delta\Theta}{\Theta_N} \right| \ll 1$$

Considering the following control law

$$\bar{u} = \frac{1}{\Lambda_N} (-\Theta_N + \vartheta) \quad (21)$$

with ϑ viewed as the new control input detailed in the sequel, one gets

$$S^{(\rho)} = \underbrace{\left(\delta\Theta - \frac{1}{\Lambda_N} \cdot \Theta_N \delta\Lambda \right)}_A + \underbrace{\left(1 + \frac{1}{\Lambda_N} \cdot \delta\Lambda \right)}_B \vartheta \quad (22)$$

Assumption 6 The internal dynamics of the system are considered bounded.

From **Assumptions 2-6**, it is obvious that the functions A and B are bounded, which means that there exists positive constants A_M, B_m and B_M such that, $\forall z \in Z$ and $t \geq 0$,

$$|A| \leq A_M, \quad 0 < B_m \leq |B| \leq B_M \quad (23)$$

5.2 Control design

Under these assumptions, s-dynamics can re-written as

$$\begin{aligned} \dot{z}_1 &= z_2 \\ &\vdots \\ \dot{z}_\rho &= a(x, t) + b(x, t) \bar{u} \end{aligned} \quad (24)$$

with $z = (z_1, \dots, z_\rho)^T = (s, \dots, s^{(\rho-1)}) \in \mathcal{Z} \subset R^\rho$

The control objective is achieved when z is evolving in a finite time around a vicinity of the origin in spite of perturbations/uncertainties. In [41], a family of higher order sliding mode controllers (HOSMCs) is designed to control (24) and is based on control Lyapunov functions (CLFs). The control law \bar{u} applied to (24) reads as

$$\begin{aligned} u &= -k_\rho [S_\rho]^\alpha \\ S_i &= [z_i]^{\frac{r_1}{r_i}} + k_{i-1}^{\frac{r_1}{r_i}} S_{i-1} \end{aligned} \quad (25)$$

with $i = 2, \dots, \rho$ and $\sigma_1 = z_1$. (k_1, \dots, k_ρ) are the controller gains where (k_2, \dots, k_ρ) can be written as a function of k_1 such that

$$\begin{aligned} k_i &= \gamma_{i-1} k_1^{\frac{\rho}{\rho-(i-1)}} \quad \forall i = 2, \dots, \rho-1 \\ B_m k_\rho - A_M &\geq \gamma_{\rho-1} k_1^\rho \end{aligned} \quad (26)$$

with the parameters γ_{i-1} , $i = 2, \dots, \rho-1$ numerically calculated to ensure the time derivative of the CLF [41] negative definite. The proposed values of γ_{i-1} for $\rho = 2, 3, 4$ are given in Table below.

ρ	Parameters		
2	$\gamma_1 = 1.26$		
3	$\gamma_2 = 9.62$	$\gamma_1 = 1.5$	
4	$\gamma_3 = 739.5$	$\gamma_2 = 8.1$	$\gamma_1 = 2$

Table 2: value of parameters γ_i

6 Adaptive FOSMC of TWT

The proposed controller, applied to system (24), reads as

$$\begin{aligned} u &= -k_\rho \lceil S_\rho \rceil^\alpha \\ S_i &= \lceil z_i \rceil^{\frac{r_1}{r_i}} + k_{i-1}^{\frac{r_1}{r_i}} S_{i-1} \end{aligned} \quad (27)$$

with (k_1, \dots, k_ρ) tuned as in (31) and α varying between 0 and 1 via the following adaptive law

$$\alpha = \max \left(-\beta \sum_{i=1}^{\rho} \frac{|z_i|}{|z_i| + \varepsilon_{z_i}} + 1, 0 \right) \quad (28)$$

Parameters $\varepsilon_{z_i}, i = 1, \dots, \rho$ and β are positive constants set by the user with $\beta > 1$.

This controller allows the establishment of a ρ^{th} -order sliding mode, i.e. z reaches zero in a finite time, where a new parameter α is introduced as an exponent(exp i) of S_ρ . The evolution of α is based on the accuracy of the closed-loop system and gives rise to an efficient trade-off between precision and energy consumption. It also allows reducing the chattering phenomenon. Note $\rho = 1$ yields classical FOSMC.

The control design described above is now applied to the twin wind turbines structure described in above Section. The control strategy is designed from the nonlinear model system given by (9). First-of-all, define the output vector

$$y = \begin{bmatrix} \sigma_{\psi-\alpha} \\ \sigma_{\Omega_1-\Omega_1^*} \\ \sigma_{i_{d,1}} \\ \sigma_{\Omega_2-\Omega_2^*} \\ \sigma_{i_{d,2}} \end{bmatrix} = \begin{bmatrix} \psi - \alpha \\ \Omega_1 - \Omega_1^* \\ i_{d,1} \\ \Omega_2 - \Omega_2^* \\ i_{d,2} \end{bmatrix} \quad (29)$$

and recall that the control objective is to force y towards 0 (in practice, this objective is to force y towards a vicinity of 0).

Structural analysis- Analysis of system (9) with output (29) gives

- The relative degree vector [29] of system (9) – (14) with output (29) and versus $\bar{u}(13)$ is $[3 \ 2 \ 1 \ 2 \ 1]^T$;

- The angle $\psi - \alpha$ and the both direct currents i_{d1} and i_{d2} are respectively controlled by $\Delta\beta, V_{d1}$ and V_{d2} ; concerning the both velocities Ω_1 and Ω_2 , their dynamics are influenced by direct and quadratic currents-there is a coupling. However, the influence of direct currents on velocities dynamics is very limited given that the direct currents are forced at 0. Then, it can be established that the coupling is very reduced and the both velocities Ω_1 and Ω_2 are finally controlled respectively by V_{q1} and V_{q2} .

Uncertainties and perturbations- The main parameters on which uncertainties have been considered, are

- The total inertia J ,
- The yaw inertia K_r ,
- The yaw dry friction D_r ,

y	i	β_i	ϵ_{i1}	ϵ_{i2}	ϵ_{i3}
$\psi - \alpha$	1	1.1	$5 * 10^{-5}$	10^{-3}	10^{-1}
$\sigma_{\Omega_1 - \Omega_1^*}$	2	11	$2 * 10^{-1}$	5	
$\sigma_{i_{d,1}}$	3	11	$3 * 10^{-3}$		
$\sigma_{\Omega_2 - \Omega_2^*}$	4	11	$2 * 10^{-1}$	5	
$\sigma_{i_{d,2}}$	5	11	$3 * 10^{-3}$		

Table 3: Controller parameters [33],[34]

According to (28), one can define $\alpha(\exp)$ parameter as,

$$\begin{aligned} \exp1 &= \max(-\beta_1 \left(\frac{|\psi - \alpha|}{|\psi - \alpha| + \epsilon_{11}} + \frac{|\dot{\psi} - \dot{\alpha}|}{|\dot{\psi} - \dot{\alpha}| + \epsilon_{12}} + \frac{|\ddot{\psi} - \ddot{\alpha}|}{|\ddot{\psi} - \ddot{\alpha}| + \epsilon_{13}} \right) + 1, 0) \\ \exp2 &= \max(-\beta_2 \left(\frac{|\Omega_1 - \Omega_1^*|}{|\Omega_1 - \Omega_1^*| + \epsilon_{21}} + \frac{|\dot{\Omega}_1 - \dot{\Omega}_1^*|}{|\dot{\Omega}_1 - \dot{\Omega}_1^*| + \epsilon_{22}} \right) + 1, 0) \\ \exp3 &= \max(-\beta_3 \left(\frac{|i_{d,1}|}{|i_{d,1}| + \epsilon_{31}} \right) + 1, 0) \\ \exp4 &= \max(-\beta_4 \left(\frac{|\Omega_2 - \Omega_2^*|}{|\Omega_2 - \Omega_2^*| + \epsilon_{41}} + \frac{|\dot{\Omega}_2 - \dot{\Omega}_2^*|}{|\dot{\Omega}_2 - \dot{\Omega}_2^*| + \epsilon_{42}} \right) + 1, 0) \\ \exp5 &= \max(-\beta_5 \left(\frac{|i_{d,2}|}{|i_{d,2}| + \epsilon_{51}} \right) + 1, 0) \end{aligned}$$

One supposes that each parameter can be written as the sum of a nominal value and an uncertain part, i.e., for example, $J = J_N + \delta J$, with J_N the nominal value of the inertia, and δJ the uncertain term. Furthermore, the aerodynamic torques Γ_{a1}, Γ_{a2} and the drag forces F_{d1}, F_{d2} can be also viewed as uncertain functions, and then can be modeled as the previous parameters (nominal and uncertain terms). Finally, all the nominal parameters/functions and their associated uncertain terms are supposed to be bounded.

From the definition of y , and given that the relative degree of each component of the sliding vector has to be equal to 1, one defines the sliding variable vector according to (24) as

$$\begin{aligned} S_{\psi - \alpha} &= \ddot{\sigma}_{\psi - \alpha}^3 \text{sign}(\ddot{\sigma}_{\psi - \alpha}) + K_{12}^3 [\dot{\sigma}_{\psi - \alpha}^{1.5} \text{sign}(\dot{\sigma}_{\psi - \alpha}) + K_{11}^{1.5} (\sigma_{\psi - \alpha})] \\ S_{\Omega_1 - \Omega_1^*} &= \dot{\sigma}_{\Omega_1 - \Omega_1^*}^2 \text{sign}(\dot{\sigma}_{\Omega_1 - \Omega_1^*}) + K_{21}^2 (\sigma_{\Omega_1 - \Omega_1^*}) \\ S_{i_{d1}} &= \sigma_{i_{d,1}} \\ S_{\Omega_2 - \Omega_2^*} &= \dot{\sigma}_{\Omega_2 - \Omega_2^*}^2 \text{sign}(\dot{\sigma}_{\Omega_2 - \Omega_2^*}) + K_{41}^2 (\sigma_{\Omega_2 - \Omega_2^*}) \\ S_{i_{d2}} &= \sigma_{i_{d,2}} \end{aligned}$$

- Then one gets,

$$\begin{bmatrix} \dot{S}_{\psi-\alpha} \\ \dot{S}_{\Omega_1-\Omega_1^*} \\ \dot{S}_{id1} \\ \dot{S}_{\Omega_2-\Omega_2^*} \\ \dot{S}_{id2} \end{bmatrix} = \varphi_1(\cdot) + \varphi_2(\cdot) \begin{bmatrix} \Delta\beta \\ V_{d_1} \\ V_{q_1} \\ V_{d_2} \\ V_{q_2} \end{bmatrix} \quad (30)$$

$$\dot{S} = \varphi_1(\cdot) + \varphi_2(\cdot).\vartheta$$

with functions $\varphi_1(\cdot)$ and $\varphi_2(\cdot)$ detailed in the sequel. The matrix φ_2 and its nominal value φ_{2N} are invertible if

$$\psi - \alpha \neq (\pm 2k + 1)\frac{\pi}{2} \quad (31)$$

with $k \in \mathbb{N}$. This condition corresponds to the case that the wind direction is not strictly parallel to the arm linking the two wind turbines. It is easy to see that, if it is the case, the system becomes not controllable because no drag forces difference can be generated. Then in the sequel, one supposes that condition (36) is fulfilled.

The matrices φ_1 and φ_2 are detailed here with $f_i, i \in \{1, 2, \dots, 7\}$ defined as

$$f_1 = \frac{p\phi_f}{J}, \quad f_2 = \frac{p(L_d - L_q)}{J}, \quad f_3 = \frac{R_s}{L_q}, \quad f_4 = \frac{pL_d}{L_q}, \quad f_5 = \frac{p\phi_f}{L_q}, \quad f_6 = \frac{R_s}{L_d}, \quad f_7 = \frac{pL_q}{L_d}$$

The time derivative of the term B and C appearing in the matrix φ_1 depends on λ, Ω, V, ψ . These derivatives are given as follows

$$\begin{aligned} \dot{B} &= \frac{\partial B}{\partial t} = \frac{\partial B}{\partial \lambda} \cdot \frac{\partial \lambda}{\partial t} = (b_1 + 2b_2\lambda + 3b_3\lambda^2) \cdot \frac{\partial}{\partial t} \left(\frac{\Omega R}{V \cos(\psi - \alpha)} \right) \\ &= (b_1 + 2b_2\lambda + 3b_3\lambda^2) \cdot \left(\frac{R}{V \cos(\psi - \alpha)} \dot{\Omega} + \lambda \operatorname{tg}(\psi - \alpha) \dot{\psi} - \frac{\lambda}{V} \dot{V} \right) \\ \dot{C} &= \frac{\partial C}{\partial t} = \frac{\partial C}{\partial V} \cdot \frac{\partial V}{\partial t} + \frac{\partial C}{\partial \psi} \cdot \frac{\partial \psi}{\partial t} \\ &= \frac{2C}{V} \dot{V} - 2 \operatorname{tg}(\psi - \alpha) \dot{\psi} \\ \varphi_1(\cdot) &= \begin{bmatrix} \left(\lambda_{1\psi} - \frac{D_r}{K_r} \right) \ddot{\psi} - \lambda_{1\psi} \ddot{\psi}^* + \lambda_{2\psi} \left(\dot{\psi} - \dot{\psi}^* \right) \dots \\ + \frac{CL}{K_r T_\beta} B (\beta_1 - \beta_2) + \frac{CL}{K_r} (\beta_1 - \beta_2) \dot{B} + \frac{BL}{K_r} (\beta_1 - \beta_2) \dot{C} \\ \frac{1}{J} \dot{\Gamma}_{a1} - (f_1 + f_2 i_{d1}) [-f_3 i_{q1} - f_4 \Omega_1 i_{d1} - f_5 \Omega_1] - f_2 i_{q1} \dots \\ [-f_6 i_{d1} + f_7 \Omega_1 i_{q1}] + \left(\lambda_{\Omega 1} - \frac{f_v}{J} \right) \dot{\Omega}_1 - \lambda_{\Omega 1} \dot{\Omega}_1^* - \ddot{\Omega}_1^* \\ - \frac{R_s}{L_d} i_{d1} + \frac{PL_q}{L_d} \Omega_1 i_{q1} \\ \frac{1}{J} \dot{\Gamma}_{a2} - (f_1 + f_2 i_{d2}) [-f_3 i_{q2} - f_4 \Omega_2 i_{d2} - f_5 \Omega_2] - f_2 i_{q2} \dots \\ [-f_6 i_{d2} + f_7 \Omega_2 i_{q2}] + \left(\lambda_{\Omega 2} - \frac{f_v}{J} \right) \dot{\Omega}_2 - \lambda_{\Omega 2} \dot{\Omega}_2^* - \ddot{\Omega}_2^* \\ - \frac{R_s}{L_d} i_{d2} + \frac{PL_q}{L_d} \Omega_2 i_{q2} \end{bmatrix} \end{aligned}$$

$$\varphi_2(.) = \begin{bmatrix} \frac{-2}{K_r T_\beta} LCB & 0 & 0 & 0 & 0 \\ 0 & \frac{-f_2}{L_d} i_{q1} & \frac{-1}{L_q} (f_1 + f_2 i_{d1}) & 0 & 0 \\ 0 & \frac{1}{L_d} & 0 & 0 & 0 \\ 0 & 0 & 0 & \frac{-f_2}{L_d} i_{q2} & \frac{-1}{L_q} (f_1 + f_2 i_{d2}) \\ 0 & 0 & 0 & \frac{1}{L_d} & 0 \end{bmatrix}$$

- Similarly the nominal and uncertain part is defined as,

$$\begin{aligned} \varphi_1 &= \varphi_{1N} + \Delta\varphi_1 \\ \varphi_2 &= \varphi_{2N} + \Delta\varphi_2 \end{aligned} \quad (32)$$

It is reasonable to consider that the parametric uncertainties have limited magnitudes with respect to the nominal values. It means that, thanks to the control law (33), dynamics of S is almost decoupled.

- The control input is defined as,

$$\begin{bmatrix} \Delta\beta \\ V_{d_1} \\ V_{q_1} \\ V_{d_2} \\ V_{q_2} \end{bmatrix} = [\varphi_{2N}(.)]^{-1} [-\varphi_{1N}(.) + \begin{bmatrix} -K_{13} S_{\psi-\alpha}^{\text{exp}1} \text{sign}(S_{\psi-\alpha}) \\ -K_{22} S_{\Omega_1-\Omega_1^*}^{\text{exp}2} \text{sign}(S_{\Omega_1-\Omega_1^*}) \\ -K_{31} S_{id1}^{\text{exp}3} \text{sign}(S_{id1}) \\ -K_{42} S_{\Omega_2-\Omega_2^*}^{\text{exp}4} \text{sign}(S_{\Omega_2-\Omega_2^*}) \\ -K_{51} S_{id2}^{\text{exp}5} \text{sign}(S_{id2}) \end{bmatrix}] \quad (33)$$

The sliding vector S converges to a vicinity of the origin in a finite time, by setting the gains sufficiently large in order to ensure the sliding condition for each component of the sliding vector.

y	i	K_{i1}	K_{i2}	K_{i3}
$\psi - \alpha$	1	0.5	0.3536	2.2025
$\sigma_{\Omega_1-\Omega_1^*}$	2	5	100	
$\sigma_{i_{d,1}}$	3	10		
$\sigma_{\Omega_2-\Omega_2^*}$	4	5	100	
$\sigma_{i_{d,1}}$	5	10		

Table 4: Gains tuned [33],[34]

6.1 Results

Simulations have been performed using MATLAB/Simulink with sampling period $\tau = 1\text{ms}$. The controller is evaluated with performances of oscillations of the electromagnetic torque, tracking of $\Omega - \Omega_{\text{ref}}$, $i_{d,i}$, turbine structure($\psi - \alpha$), as well as the mean power generated. The gains chosen are from the Table 4.

In order to test the robustness of the controller to the parametric uncertainties, following variations have been done:

Parametric uncertainties of PMSG	
Resistance(R)	20%
Inductance (L_d)	20%
Pitch angle β_i	50%
Drag coefficient $C_{d,i}$	50%

As previously mentioned, the computation of $\varphi_1(\cdot)$ that is required for ϑ , needs the knowledge of Γ_1^* and Γ_2^* . In fact, it is necessary to compute estimated values of $\dot{\psi}, \ddot{\psi}, \dot{\Omega}_i$. The first and second derivatives are estimated by a filter defines as $\frac{s}{\tau s+1}$ with $\tau = 1/60$.

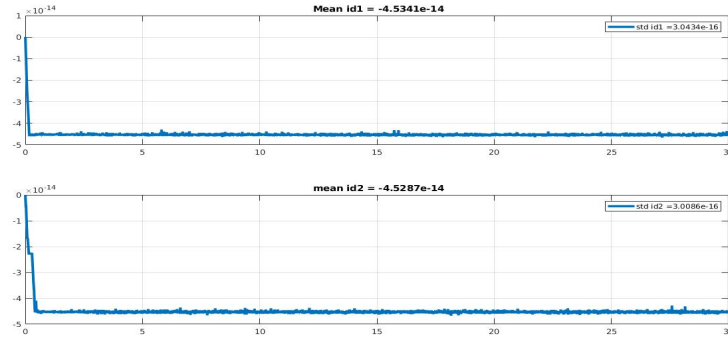


Figure 5: Currents tracking

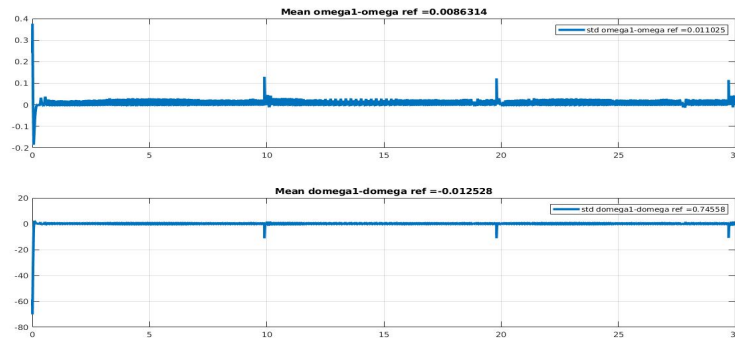


Figure 6: Ω_1 tracking

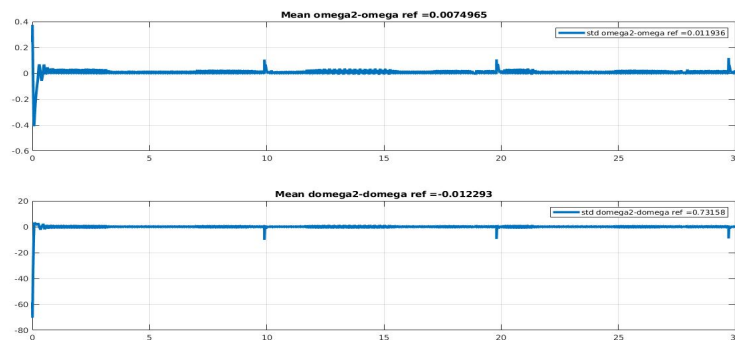


Figure 7: Ω_2 tracking

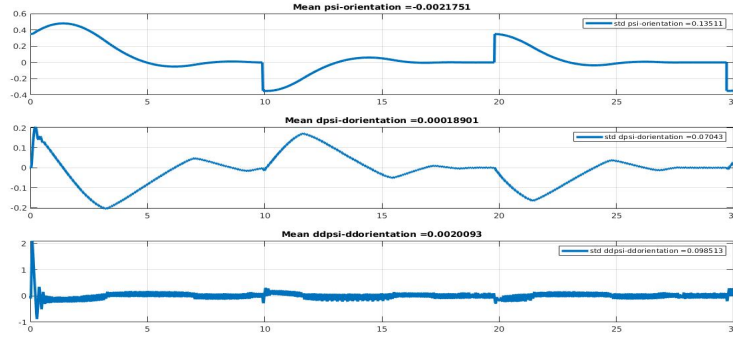


Figure 8: $\psi - \alpha$ and its derivatives

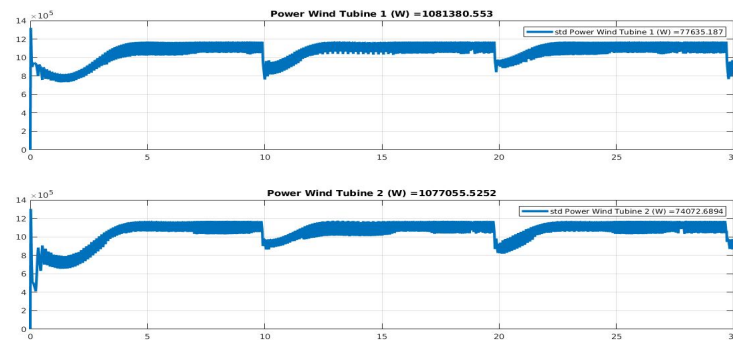


Figure 9: Mean power

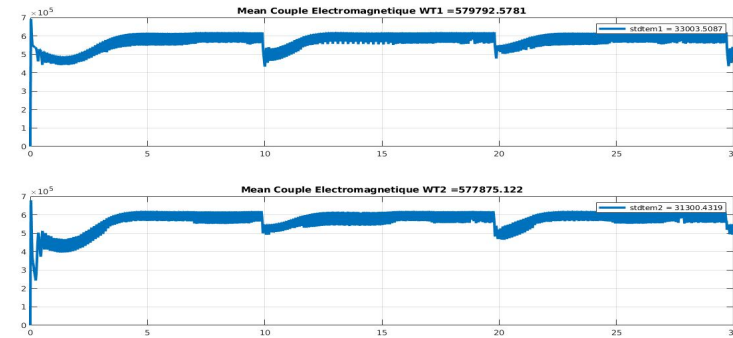


Figure 10: Γ_{em} tracking

At $t = 20$ and 30 sec, the sudden loss of power is due to loss in torque which is in due to change in wind direction, which causes the misalignment between the structure and wind direction. In practical applications of sliding mode control, engineers experience undesirable phenomenon of oscillation having a finite frequency and amplitude, which is known as '**chattering**' in Figure 6, 9 and 10. An indicator used to quantify the chattering effect is the standard deviation.

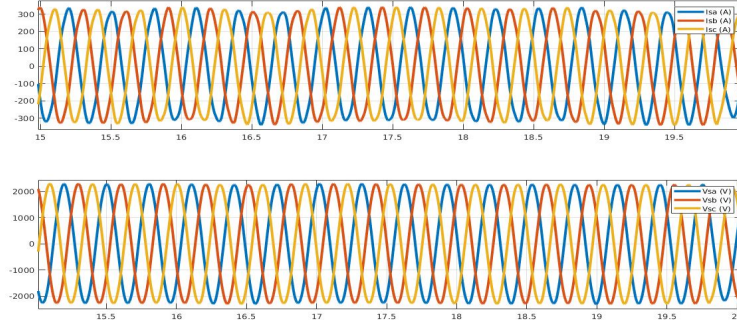


Figure 11: 3 phase voltage and currents

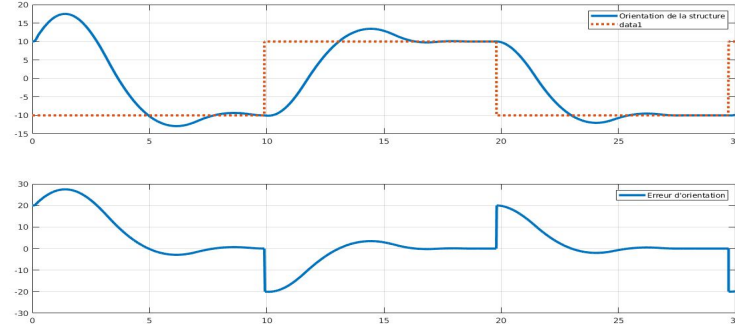


Figure 12: $\psi - \alpha$ tracking

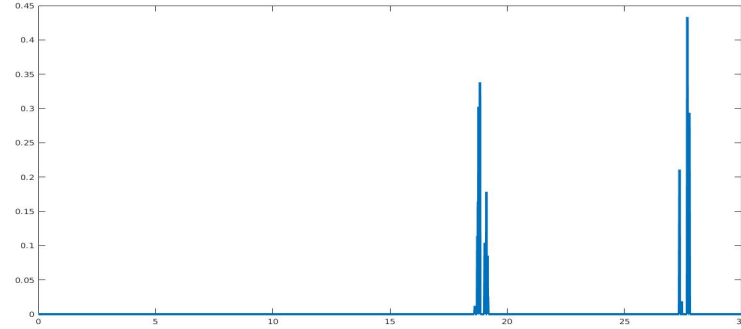


Figure 13: exponent(α) of $\psi - \alpha$

Initially the value of $\exp(\alpha)$ for structure orientation($\psi - \alpha$) is equal to zero(see Figure 13) this is because the yaw angle ψ does not track the wind direction α ; hence, $\exp(\alpha) = 0$ forcing ψ to α . When the latter is achieved and a steady state is attained ($15 < t < 20$ sec) and ($25 < t < 30$ sec), then $\exp(\alpha)$ starts varying between 0 and 1 reducing the chattering phenomenon and also reducing the control effort. A similar logic can be applied

to $\exp(\alpha)$ of $i_{d,i}$, always equal to 1 almost all the time, it means that the direct currents are not affected by the uncertainties considered in this simulation.

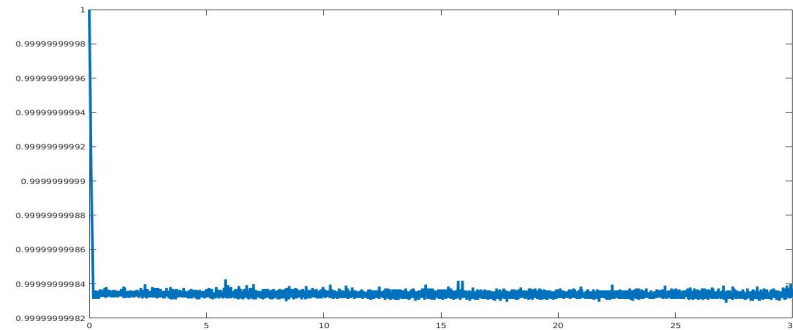


Figure 14: $\exp(\alpha)$ of $i_{d,1}$

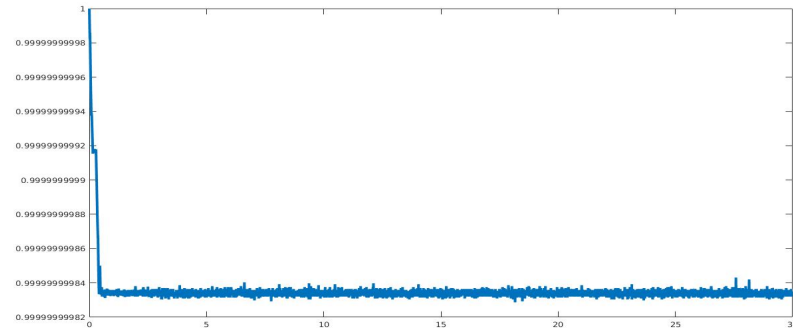


Figure 15: $\exp(\alpha)$ of $i_{d,2}$

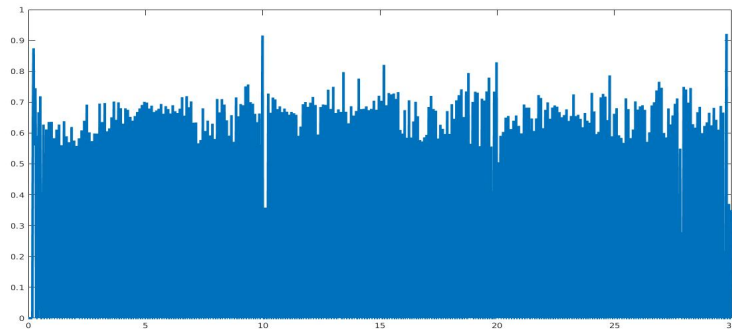


Figure 16: $\exp(\alpha)$ of Ω_1

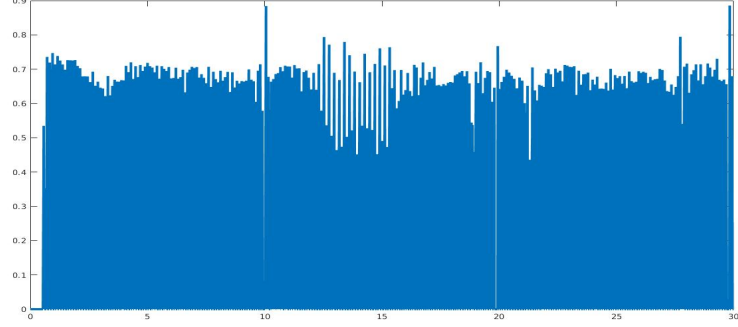


Figure 17: exponent(α) of Ω_2

7 Differentiator

A very recent differentiator [9] is used in order to provide an estimation of the differentiated signal that is both smooth, accurate, and not too sensible to the noise measurement. In fact, the differentiator is linear in case of large high frequency noise on the measurement, and is based on super-twisting algorithm when the noise is reduced; this feature is made thanks to the use of a high-pass filter. The super twisting differentiator ($\alpha = 0.5$) is not sensible to perturbation but its accuracy is degraded when the signal is affected by the noise. The linear differentiator ($\alpha = 1$) has better property in the presence of noise but is less robust to perturbations. The estimated signal is a trade-off between the exact differentiator and linear differentiator.

Denoting y_m the signal that has to be differentiated, the differentiator providing an estimation of the first order time derivative of y_m denoted z_2 , reads as [9]

$$\begin{aligned}\dot{z}_1 &= z_2 + k_1 \mu |y_m - z_1|^\gamma \operatorname{sign}(y_m - z_1) \\ \dot{z}_2 &= k_2 \gamma \mu^2 |y_m - z_1|^{2\gamma-1} \operatorname{sign}(y_m - z_1)\end{aligned}\tag{34}$$

with γ derived from the following low-pass filter

$$\begin{aligned}\dot{z}_3 &= -\tau z_3 + \tau |y_{mhf}| \\ \gamma &= \frac{1}{2} \left(1 + \frac{z_3}{z_3 + \epsilon} \right)\end{aligned}\tag{35}$$

The signal y_{mhf} is derived from a high-pass filter with y_m as its input, and ω_c its cut-off frequency denoted, and reads as (s being the Laplace complex variable, Y_{mhf} (resp. Y_m) the Laplace transform of y_{mhf} (resp. y_m), and $s_c = \frac{s}{\omega_c}$)

$$Y_{mhf} = \frac{s_c^4}{(s_c^2 + 0.7654s_c + 1)(s_c^2 + 1.8478s_c + 1)} Y_m\tag{36}$$

The concept of this differentiator is the following: when the signal that must be differentiated, is noisy, a linear differentiator ($\gamma = 1$) must be applied in order to limit the level of noise introduced in the controller. At the opposite, when the signal is free of noise, an exact differentiator ($\gamma = 0.5$) is applied. Thanks to the time-varying parameter γ versus the level of noise on the measurement, the differentiator (39) provides an estimation z_2 of \dot{y}_m (whereas z_1 is a filtered estimation of the noise free measurement). The idea of this differentiator is based on the following items

- the filter (36) is a high pass Butterworth filter used to "estimate" the magnitude of the high frequency part of y_m . The idea consists of "detecting" if there is high frequency components (as noise) that could be amplified by the differentiator. This filter provides y_{mhf}

- if the signal y_m is free of noise, an exact differentiation can be made by stating γ to 0.5, i.e. by using super-twisting algorithm. In this case, the signal y_{mhf} is low, that gives z_3 tending towards 0 . Then, γ tends towards 0.5 with a dynamics tuned by the parameter τ ;
- if the signal y_m is noisy, an exact differentiation would engender high level of oscillations in the control; it is the reason why a linear differentiator has to be applied. In this case, the signal y_{mhf} is high, that gives a high value for z_3 . Then, γ tends towards 1 : based on (34), a linear differentiator is applied.

The role of each parameter of the differentiator is detailed in [42] and is quickly recalled here

- $\mu > 0(34)$ has to be chosen large enough to ensure the convergence of z_1 towards y_m ;
- $\epsilon > 0(35)$ has to be chosen not too large in order to ensure $\gamma \rightarrow 1$ (resp. 0.5) when the signal y_m is free of noise (resp. noisy), i.e. when z_3 tends to 0 (resp. ∞) ;
- $\tau > 0(35)$ acts on the dynamics of z_3 and γ . It has to be chosen sufficiently small in order to make the parameter γ sufficiently reactive;
- ω_c is the cut-off frequency of the filter (36) and has to be chosen sufficiently large versus y_m -dynamics.

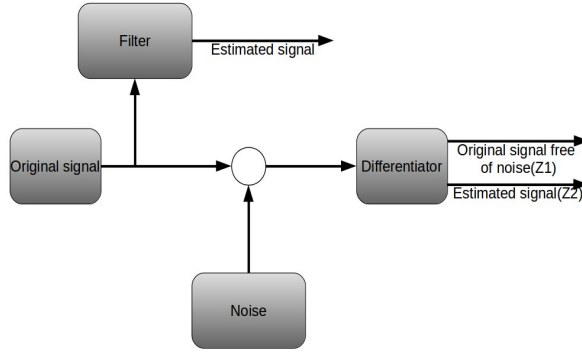


Figure 18: Differentiator scheme of the SEREO structure

7.1 Results

In order to check the behavior of the closed-loop system with noise, a white noise is introduced. Now the wind speed is modeled as

$$V = V_m + V_d$$

where V_m is the original signal(wind speed) with 10 m/s and V_d is a time-varying term defined as a white noise. Characteristics of white noise, noise power - 0.1, sampling time - 0.01 sec, speed - [23341]. During the simulation the Differentiator [9],[10] was considered in the loop. The following results are comparison between the filter $\frac{s}{\tau s+1}$ and the differentiator [9],[10]. The tuned gains for the differentiator is given below.

Parameters	Wind speed	Ω, ψ
K_1	10	10
K_2	2	40
μ	10	20
τ	0.01	0.05
ϵ	0.001	0.01

Table 5: Tuned Gains

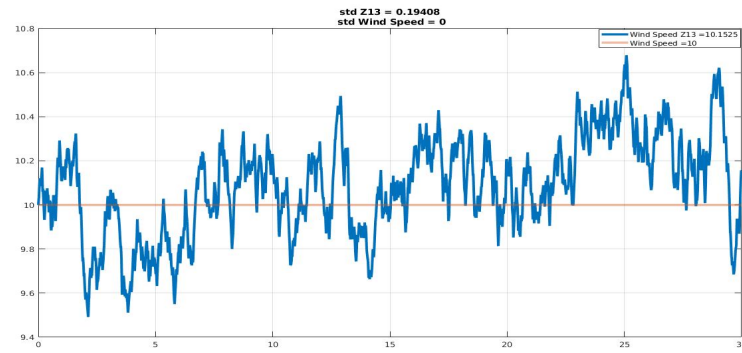


Figure 19: Wind speed(V) Original signal vs Differentiator(in-loop)

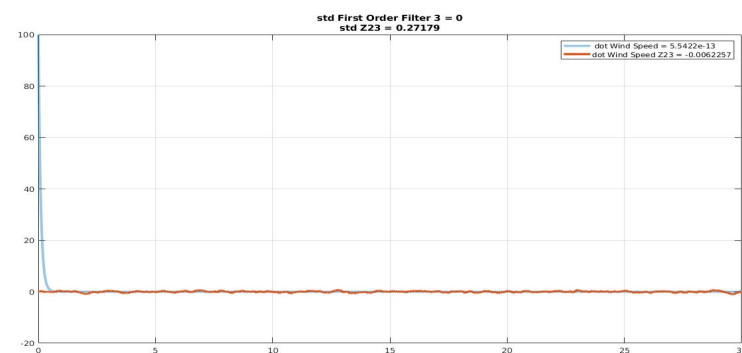


Figure 20: Wind speed(\dot{V}) Filter vs Differentiator(in-loop)



Figure 21: Wind speed(\dot{V}) Filter vs Differentiator(in-loop)(zoom)

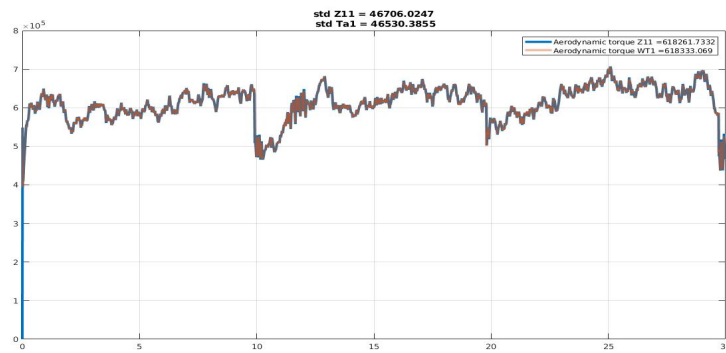


Figure 22: Aerodynamic torque Γ_{a1} Original signal vs Differentiator(in-loop)

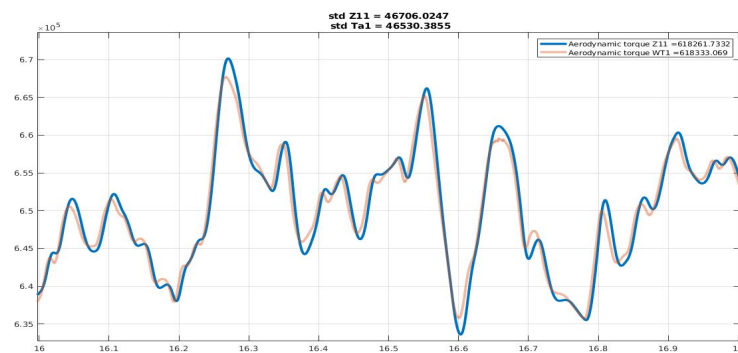


Figure 23: Aerodynamic torque Γ_{a1} Original signal vs Differentiator(in-loop)(zoom)

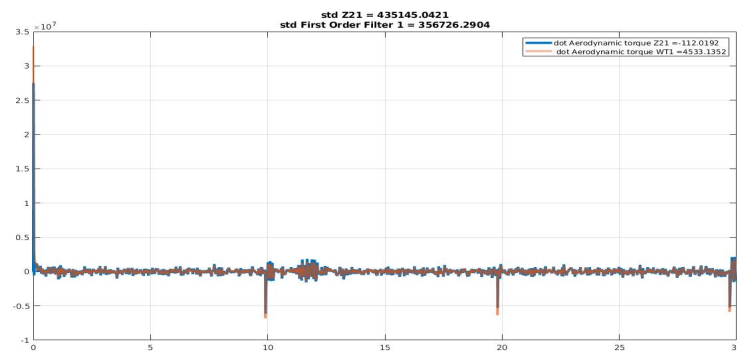


Figure 24: $\dot{\Gamma}_{a1}$ Filter vs Differentiator(in-loop)

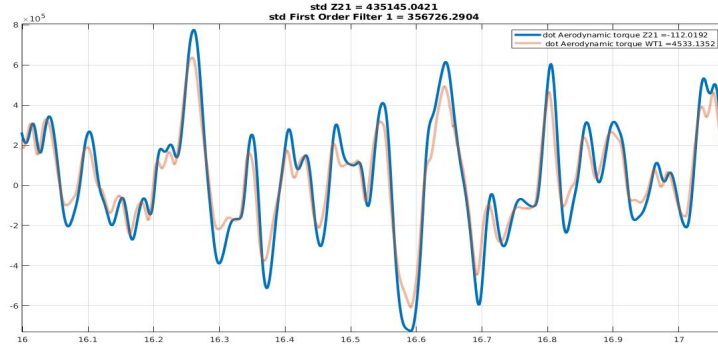


Figure 25: $\dot{\Gamma}_{a1}$ Filter vs Differentiator(in-loop)(zoom)

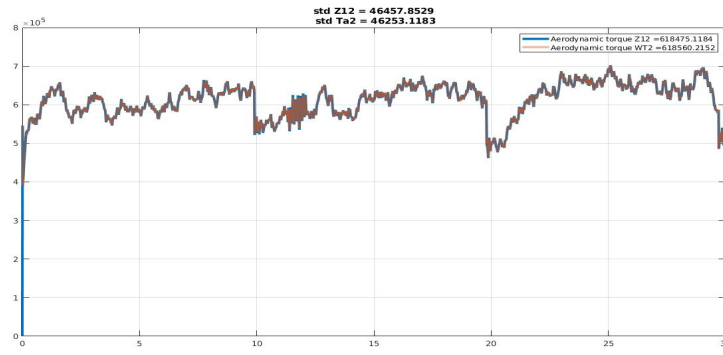


Figure 26: Γ_{a2} Original signal vs Differentiator(in-loop)

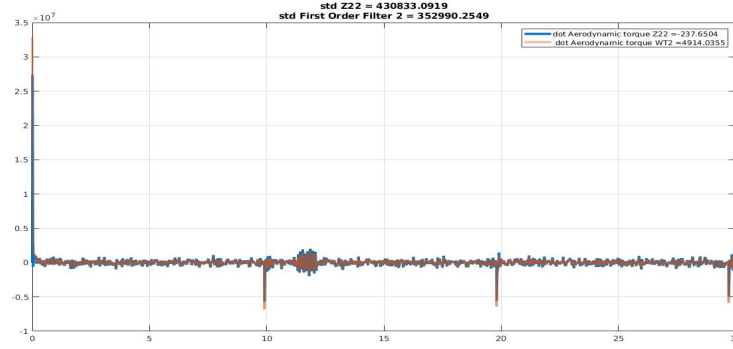


Figure 27: $\dot{\Gamma}_{a2}$ Filter vs Differentiator(in-loop)

The estimated signal of \dot{V} and $\dot{\Gamma}$ from the differentiator are acceptable, from here on the differentiator is used to estimate the signal. For simplicity, for the following experiments no noise is considered.

8 Adaptive HOSMC of TWT

From the above results, the electromagnetic torque has a high frequency of oscillation with constant amplitude. These oscillations can be minimized by acting on higher derivatives of direct and quadratic voltages of Ω . In this section HOSMC is applied only to Ω . Note $\rho = 2$ yields HOSMC.

$$\ddot{S}_{\Omega-\Omega^*} = \varphi_1(\cdot) + \varphi_2(\cdot) \begin{bmatrix} \dot{V}_d \\ \dot{V}_q \end{bmatrix}$$

So the new input for Ω tracking are \dot{V}_d and \dot{V}_q . V_d and V_q act as a system states now. The new input vector is defined as $[\Delta\beta \quad \dot{V}_{d_1} \quad \dot{V}_{q_1} \quad \dot{V}_{d_2} \quad \dot{V}_{q_2}]^T$. The relative degree of the system is now given as $[3 \quad 3 \quad 1 \quad 3 \quad 1]^T$, one defines the sliding vector according to (25) as

$$\begin{aligned} S_{\psi-\alpha} &= \ddot{\sigma}_{\psi-\alpha}^3 \text{sign}(\ddot{\sigma}_{\psi-\alpha}) + K_{12}^3 [\dot{\sigma}_{\psi-\alpha}^{1.5} \text{sign}(\dot{\sigma}_{\psi-\alpha}) + K_{11}^{1.5}(\sigma_{\psi-\alpha})] \\ S_{\Omega_1-\Omega_1^*} &= \ddot{\sigma}_{\Omega_1-\Omega_1^*}^3 \text{sign}(\ddot{\sigma}_{\Omega_1-\Omega_1^*}) + K_{22}^3 [\dot{\sigma}_{\Omega_1-\Omega_1^*}^{1.5} \text{sign}(\dot{\sigma}_{\Omega_1-\Omega_1^*}) + K_{21}^{1.5}(\sigma_{\Omega_1-\Omega_1^*})] \\ S_{id1} &= \sigma_{i_{d,1}} \\ S_{\Omega_2-\Omega_2^*} &= \ddot{\sigma}_{\Omega_2-\Omega_2^*}^3 \text{sign}(\ddot{\sigma}_{\Omega_2-\Omega_2^*}) + K_{42}^3 [\dot{\sigma}_{\Omega_2-\Omega_2^*}^{1.5} \text{sign}(\dot{\sigma}_{\Omega_2-\Omega_2^*}) + K_{41}^{1.5}(\sigma_{\Omega_2-\Omega_2^*})] \\ S_{id2} &= \sigma_{i_{d,2}} \end{aligned}$$

The sliding vector has to admit the relative degree 1. Then one gets,

$$\begin{bmatrix} \dot{S}_{\psi-\alpha} \\ \dot{S}_{\Omega_1-\Omega_1^*} \\ \dot{S}_{id1} \\ \dot{S}_{\Omega_2-\Omega_2^*} \\ \dot{S}_{id2} \end{bmatrix} = \bar{\varphi}_1(\cdot) + \bar{\varphi}_2(\cdot) \begin{bmatrix} \Delta\beta \\ \dot{V}_{d_1} \\ \dot{V}_{q_1} \\ \dot{V}_{d_2} \\ \dot{V}_{q_2} \end{bmatrix} \quad (37)$$

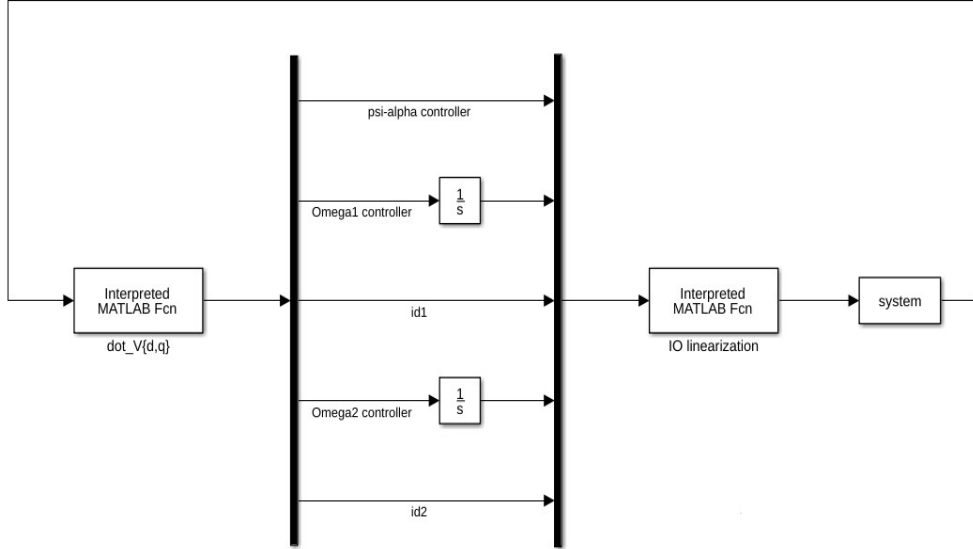


Figure 28: Control scheme for HOSMC

With the function $\bar{\varphi}_1(\cdot)$ and $\bar{\varphi}_2(\cdot)$ defined in the sequel,

$$\begin{aligned}
& \left[\begin{aligned}
& \left(\lambda_{1\psi} - \frac{D_r}{K_r} \right) \ddot{\psi} - \lambda_{1\psi} \dot{\psi}^* + \lambda_{2\psi} \left(\dot{\psi} - \dot{\psi}^* \right) + \frac{CL}{K_r T_\beta} B (\beta_1 - \beta_2) + \frac{CL}{K_r} (\beta_1 - \beta_2) \dot{B} + \frac{BL}{K_r} (\beta_1 - \beta_2) \dot{C} \\
& \quad + \Omega_1 i_{d1} \left(-2f_2 f_3 f_6 - f_3^2 f_2 - f_1 f_5 f_2 - f_2 f_6^2 - f_1^2 f_4 - \frac{f_1 f_5 f_2}{J} - \frac{f_3 f_2 f_v}{J} \right. \\
& \quad \left. - \frac{f_v f_2 f_6}{J} - \frac{f_2 f_v^2}{J^2} \right) + \Omega_1 i_{d1}^2 \left(-3f_2 f_4 f_6 - f_2 f_3 f_4 - \frac{2f_2 f_4 f_v}{J} \right) - \frac{\dot{\Omega}_1 f_v}{J^2} \\
& \quad + \Omega_1 i_{d1} \left(-2f_2 f_5 f_6 - f_2 f_3 f_5 - f_1 f_3 f_4 - f_4 f_6 f_1 - \frac{2f_1 f_4 f_v}{J} - \frac{2f_2 f_5 f_v}{J} \right) + V_{q1} i_{d1} \left(\frac{2f_2 f_6}{L_q} + \frac{f_2 f_3}{L_q} \right. \\
& \quad \left. + \frac{f_v f_2}{J L_q} \right) + \Omega_1 i_{q1}^2 \left(3f_2 f_3 f_7 + f_2 f_6 f_7 + \frac{2f_2 f_7 f_v}{J} \right) + \Omega_1^2 i_{q1} i_{d1} \left(4f_2 f_4 f_7 \right) + \Omega_1^2 i_{q1} \left(3f_2 f_5 f_7 \right. \\
& \quad \left. + f_1 f_4 f_7 \right) + \Omega_1 i_{q1} V_{q1} \left(\frac{-3f_2 f_7}{L_q} \right) + V_{d1} i_{q1} \left(\frac{2f_2 f_3}{L_d} + \frac{f_2 f_v}{J L_d} + \frac{f_2 f_6}{L_d} \right) + V_{d1} i_{d1} \Omega_1 \left(\frac{3f_2 f_4}{L_d} \right) \\
& \quad + V_{d1} \Omega_1 \left(\frac{2f_2 f_5}{L_d} + \frac{f_1 f_4}{L_d} \right) + V_{d1} V_{q1} \left(\frac{-2f_2}{L_d L_q} \right) + i_{d1}^2 \Gamma_{a1} \left(\frac{f_2 f_4}{J} \right) + i_{d1}^3 i_{q1} \left(-f_2^2 f_4 \right) + i_{d1}^2 i_{q1} \left(-2f_1 f_2 f_4 - f_2^2 f_5 \right) \\
& \quad + \Gamma_{a1} \left(\frac{f_v^2}{J^3} + \frac{f_1 f_5}{J^3} \right) + i_{q1} \left(-f_1 f_3^2 - f_1^2 f_5 - \frac{f_1 f_3 f_v}{J} - \frac{f_v^2 f_1}{J^2} \right) + \Omega_1 \left(\frac{-2f_1 f_5 f_v}{J} \right. \\
& \quad \left. - f_1 f_3 f_5 - \frac{f_v^3}{J^3} \right) + V_{q1} \left(\frac{f_1 f_3}{L_q} + \frac{f_1 f_v}{J L_q} \right) + i_{q1}^2 \Gamma_{a1} \left(\frac{-f_2 f_7}{J} \right) + i_{q1}^3 i_{d1} \left(f_7 f_2^2 \right) \\
& \quad + i_{q1}^3 \left(f_1 f_2 f_7 \right) + i_{d1} \Gamma_{a1} \left(\frac{f_2 f_5 + f_1 f_4}{J} \right) - \frac{\lambda_{opt}}{R_s} \left(\cos(\psi - \alpha) (-3V\dot{\psi}^2 - 3V\dot{\psi}\ddot{\psi}) + \sin(\psi - \alpha) (-3V\ddot{\psi} - 3V\dot{\psi} + V\dot{\psi}^3 - V\ddot{\psi}) \right) \\
& \quad \bar{\varphi}_1(\cdot) = \left[\begin{aligned}
& \frac{-R_s}{L_d} i_{d1} + \frac{PL_q}{L_d} \Omega_1 i_{q1} + \frac{1}{L_d} V_{d1} \\
& \quad + \frac{\dot{\Omega}_1 f_v}{J^2} + i_{d2} i_{q2} \left(-2f_2 f_3 f_6 - f_3^2 f_2 - f_1 f_5 f_2 - f_2 f_6^2 - f_1^2 f_4 - \frac{f_1 f_5 f_2}{J} - \frac{f_3 f_2 f_v}{J} \right. \\
& \quad \left. - \frac{f_v f_2 f_6}{J} - \frac{f_2 f_v^2}{J^2} \right) + \Omega_2 i_{d2}^2 \left(-3f_2 f_4 f_6 - f_2 f_3 f_4 - \frac{2f_2 f_4 f_v}{J} \right) - \frac{\dot{\Omega}_2 f_v}{J^2} \\
& \quad + \Omega_2 i_{d2} \left(-2f_2 f_5 f_6 - f_2 f_3 f_5 - f_1 f_3 f_4 - f_4 f_6 f_1 - \frac{2f_1 f_4 f_v}{J} - \frac{2f_2 f_5 f_v}{J} \right) + V_{q2} i_{d2} \left(\frac{2f_2 f_6}{L_q} + \frac{f_2 f_3}{L_q} \right. \\
& \quad \left. + \frac{f_v f_2}{J L_q} \right) + \Omega_2 i_{q2}^2 \left(3f_2 f_3 f_7 + f_2 f_6 f_7 + \frac{2f_2 f_7 f_v}{J} \right) + \Omega_2^2 i_{q2} i_{d2} \left(4f_2 f_4 f_7 \right) + \Omega_2^2 i_{q2} \left(3f_2 f_5 f_7 \right. \\
& \quad \left. + f_1 f_4 f_7 \right) + \Omega_2 i_{q2} V_{q2} \left(\frac{-3f_2 f_7}{L_q} \right) + V_{d2} i_{q2} \left(\frac{2f_2 f_3}{L_d} + \frac{f_2 f_v}{J L_d} + \frac{f_2 f_6}{L_d} \right) + V_{d2} i_{d2} \Omega_2 \left(\frac{3f_2 f_4}{L_d} \right) \\
& \quad + V_{d2} \Omega_2 \left(\frac{2f_2 f_5}{L_d} + \frac{f_1 f_4}{L_d} \right) + V_{d2} V_{q2} \left(\frac{-2f_2}{L_d L_q} \right) + i_{d2}^2 \Gamma_{a2} \left(\frac{f_2 f_4}{J} \right) + i_{d2}^3 i_{q2} \left(-f_2^2 f_4 \right) + i_{d2}^2 i_{q2} \left(-2f_1 f_2 f_4 - f_2^2 f_5 \right) \\
& \quad + \Gamma_{a2} \left(\frac{f_v^2}{J^3} + \frac{f_1 f_5}{J^3} \right) + i_{q2} \left(-f_1 f_3^2 - f_1^2 f_5 - \frac{f_1 f_3 f_v}{J} - \frac{f_v^2 f_1}{J^2} \right) + \Omega_2 \left(\frac{-2f_1 f_5 f_v}{J} \right. \\
& \quad \left. - f_1 f_3 f_5 - \frac{f_v^3}{J^3} \right) + V_{q2} \left(\frac{f_1 f_3}{L_q} + \frac{f_1 f_v}{J L_q} \right) + i_{q2}^2 \Gamma_{a2} \left(\frac{-f_2 f_7}{J} \right) + i_{q2}^3 i_{d2} \left(f_7 f_2^2 \right) \\
& \quad + i_{q2}^3 \left(f_1 f_2 f_7 \right) + i_{d2} \Gamma_{a2} \left(\frac{f_2 f_5 + f_1 f_4}{J} \right) - \frac{\lambda_{opt}}{R_s} \left(\cos(\psi - \alpha) (-3V\dot{\psi}^2 - 3V\dot{\psi}\ddot{\psi}) + \sin(\psi - \alpha) (-3V\ddot{\psi} - 3V\dot{\psi} + V\dot{\psi}^3 - V\ddot{\psi}) \right) \\
& \quad \bar{\varphi}_2(\cdot) = \left[\begin{array}{ccccc}
\frac{-2}{K_r T_\beta} LCB & 0 & 0 & 0 & 0 \\
0 & \frac{-f_2}{L_d} i_{q1} & \frac{-1}{L_q} (f_1 + f_2 i_{d1}) & 0 & 0 \\
0 & 0 & 0 & 0 & 0 \\
0 & 0 & 0 & \frac{-f_2}{L_d} i_{q2} & \frac{-1}{L_q} (f_1 + f_2 i_{d2}) \\
0 & 0 & 0 & 0 & 0
\end{array} \right] \end{aligned} \right] \quad (38)
\end{aligned}$$

The control input is defined as,

$$\begin{aligned}
& \left[\begin{array}{c} \Delta\beta \\ V_{d1} \\ V_{q1} \\ V_{d2} \\ V_{q2} \end{array} \right] = [\bar{\varphi}_2(\cdot)]^{-1} [-\bar{\varphi}_1(\cdot) + \left[\begin{array}{c} -K_{13} S_{\psi-\alpha} \exp^1 sign(S_{\psi-\alpha}) \\ -\int K_{23} S_{\Omega_1-\Omega_2} \exp^2 sign(S_{\Omega_1-\Omega_2}) \\ -K_{31} S_{id1} \exp^3 sign(S_{id1}) \\ -\int K_{43} S_{\Omega_2-\Omega_2} \exp^4 sign(S_{\Omega_2-\Omega_2}) \\ -K_{51} S_{id2} \exp^5 sign(S_{id2}) \end{array} \right]] \quad (39)
\end{aligned}$$

Here the pre-feedback $\varphi_1(\cdot)$ and $\varphi_2(\cdot)$ is not changed to the new $\bar{\varphi}_1(\cdot)$ and $\bar{\varphi}_2(\cdot)$. The pre-feedback is kept same as the one for FOSMC, only the controller is changed for HOSMC. It is also beneficial to reduce the computation and to avoid human errors in the equations.

$$\begin{bmatrix} \Delta\beta \\ V_{d_1} \\ V_{q_1} \\ V_{d_2} \\ V_{q_2} \end{bmatrix} = [\varphi_2(\cdot)]^{-1}[-\varphi_1(\cdot) + \begin{bmatrix} -K_{13}S_{\psi-\alpha}^{\text{exp } 1}\text{sign}(S_{\psi-\alpha}) \\ -\int K_{23}S_{\Omega_1-\Omega_1^*}^{\text{exp } 2}\text{sign}(S_{\Omega_1-\Omega_1^*}) \\ -K_{31}S_{id1}^{\text{exp } 3}\text{sign}(S_{id1}) \\ -\int K_{43}S_{\Omega_2-\Omega_2^*}^{\text{exp } 4}\text{sign}(S_{\Omega_2-\Omega_2^*}) \\ -K_{51}S_{id2}^{\text{exp } 5}\text{sign}(S_{id2}) \end{bmatrix}] \quad (40)$$

Gains are tuned according to (26).

y	i	K_{i1}	K_{i2}	K_{i3}
$\psi - \alpha$	1	0.5	0.3536	2.2025
$\sigma_{\Omega_1-\Omega_1^*}$	2	44.8140	450	901877.0833
$\sigma_{i_{d,1}}$	3	10		
$\sigma_{\Omega_2-\Omega_2^*}$	4	44.8140	450	901877.0833
$\sigma_{i_{d,1}}$	5	10		

Table 6: Gains tuned [33],[34]

y	i	β_i	ϵ_{i1}	ϵ_{i2}	ϵ_{i3}
$\psi - \alpha$	1	1.1	$5 * 10^{-5}$	10^{-3}	10^{-1}
$\sigma_{\Omega_1-\Omega_1^*}$	2	11	$2 * 10^{-2}$	$3 * 10^{-2}$	0.1
$\sigma_{i_{d,1}}$	3	11	$3 * 10^{-3}$		
$\sigma_{\Omega_2-\Omega_2^*}$	4	11	$2 * 10^{-2}$	$3 * 10^{-2}$	0.1
$\sigma_{i_{d,2}}$	5	11	$3 * 10^{-3}$		

Table 7: Controller parameters [33],[34]

According to (28), one can define $\alpha(\text{exp})$ parameter as,

$$\begin{aligned} \text{exp1} &= \max(-\beta_1(\frac{|\psi - \alpha|}{|\psi - \alpha| + \epsilon_{11}} + \frac{|\dot{\psi} - \dot{\alpha}|}{|\dot{\psi} - \dot{\alpha}| + \epsilon_{12}} + \frac{|\ddot{\psi} - \ddot{\alpha}|}{|\ddot{\psi} - \ddot{\alpha}| + \epsilon_{13}}) + 1, 0) \\ \text{exp2} &= \max(-\beta_2(\frac{|\Omega_1 - \Omega_1^*|}{|\Omega_1 - \Omega_1^*| + \epsilon_{21}} + \frac{|\dot{\Omega}_1 - \dot{\Omega}_1^*|}{|\dot{\Omega}_1 - \dot{\Omega}_1^*| + \epsilon_{22}} + \frac{|\ddot{\Omega}_1 - \ddot{\Omega}_1^*|}{|\ddot{\Omega}_1 - \ddot{\Omega}_1^*| + \epsilon_{23}}) + 1, 0) \\ \text{exp3} &= \max(-\beta_3(\frac{|i_{d,1}|}{|i_{d,1}| + \epsilon_{31}}) + 1, 0) \\ \text{exp4} &= \max(-\beta_4(\frac{|\Omega_2 - \Omega_2^*|}{|\Omega_2 - \Omega_2^*| + \epsilon_{41}} + \frac{|\dot{\Omega}_2 - \dot{\Omega}_2^*|}{|\dot{\Omega}_2 - \dot{\Omega}_2^*| + \epsilon_{42}} + \frac{|\ddot{\Omega}_2 - \ddot{\Omega}_2^*|}{|\ddot{\Omega}_2 - \ddot{\Omega}_2^*| + \epsilon_{43}}) + 1, 0) \\ \text{exp5} &= \max(-\beta_5(\frac{|i_{d,2}|}{|i_{d,2}| + \epsilon_{51}}) + 1, 0) \end{aligned}$$

8.1 Results

The following results are obtained with HOSMC of Ω . HOSMC cannot eliminate **chattering** completely, but it reduces up to large extent. see in Figure 30, 31, 33, 34.

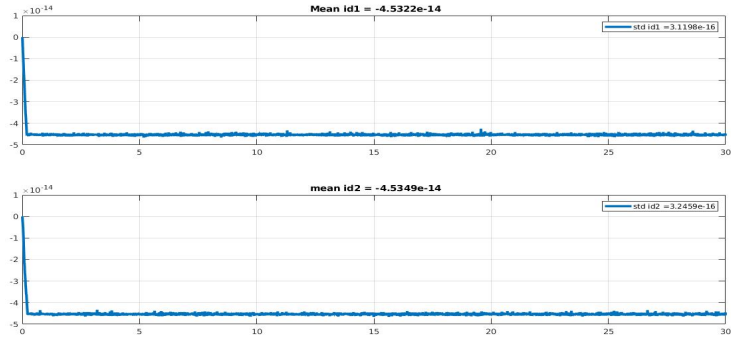


Figure 29: Currents with Differentiator in-loop

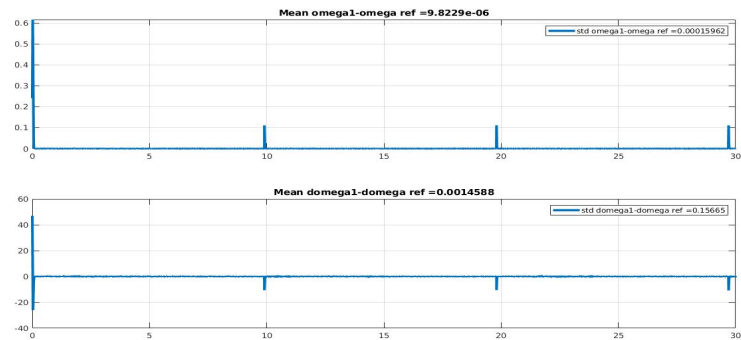


Figure 30: Ω_1 tracking with Differentiator in-loop

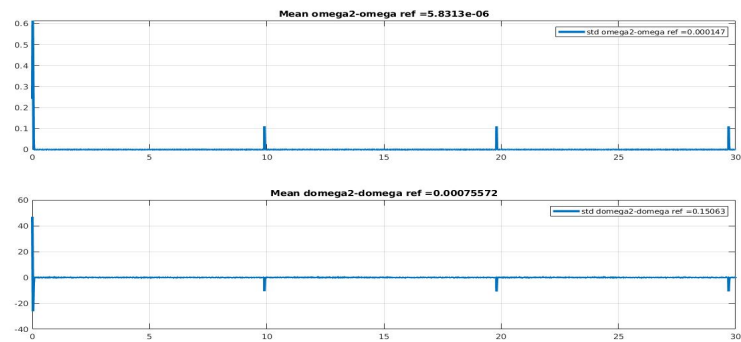


Figure 31: Ω_2 tracking with Differentiator in-loop

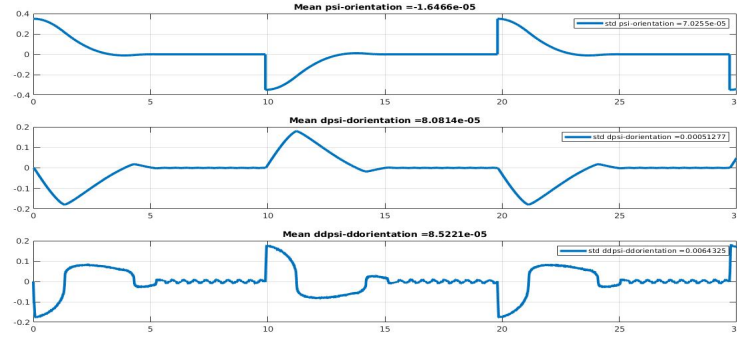


Figure 32: $\psi - \alpha$ and its derivatives with Differentiator in-loop

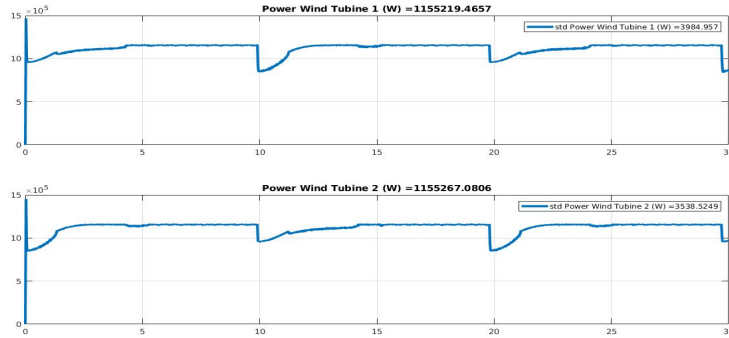


Figure 33: Power with Differentiator in-loop

Initially, we see sudden rise in mean power generated. With the larger gains the **chattering** can be reduced to larger extent, but the problem is initial sudden rise in power. Such phenomenon in Observation is referred to "**Peaking phenomenon**".

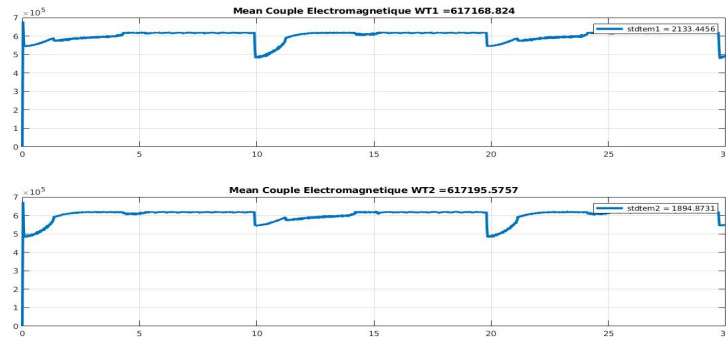


Figure 34: Γ tracking with Differentiator in-loop

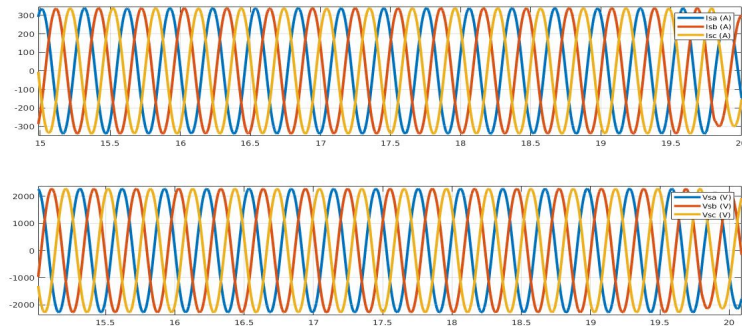


Figure 35: 3 phase voltage and currents with Differentiator in-loop

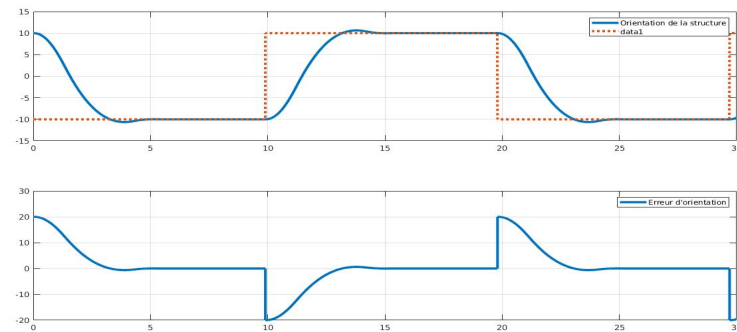


Figure 36: $\psi - \alpha$ tracking with Differentiator in-loop

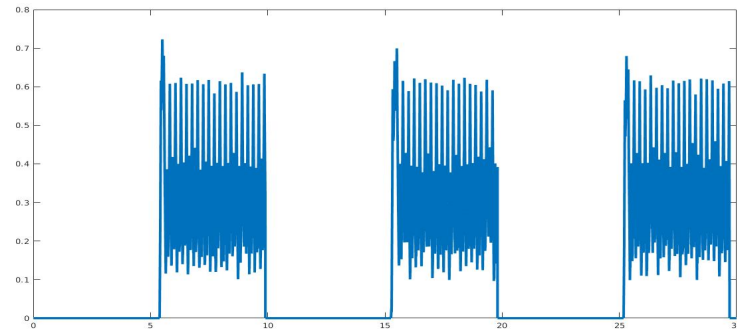


Figure 37: exponent(α) of $\psi - \alpha$

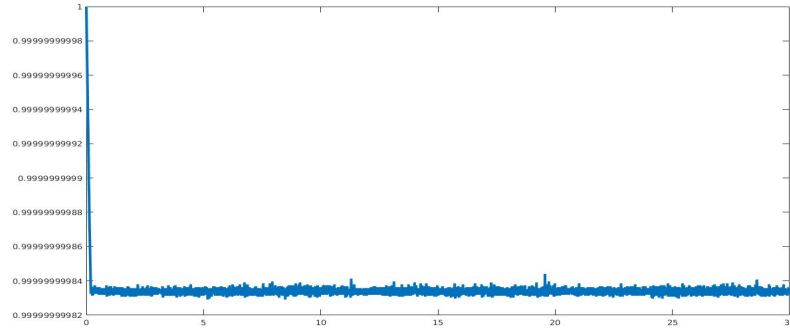


Figure 38: $\text{exponent}(\alpha)$ of $i_{d,1}$

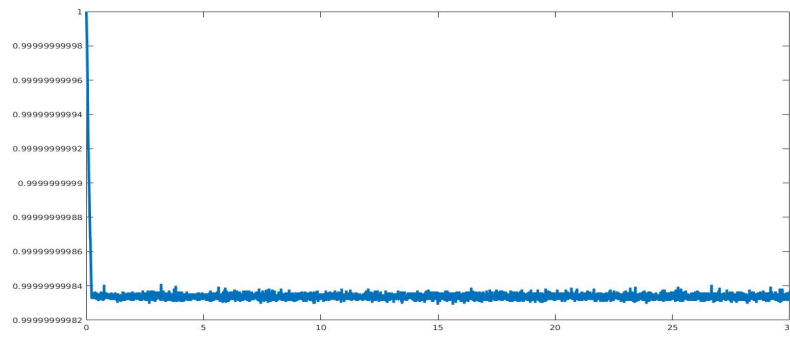


Figure 39: $\text{exponent}(\alpha)$ of $i_{d,2}$

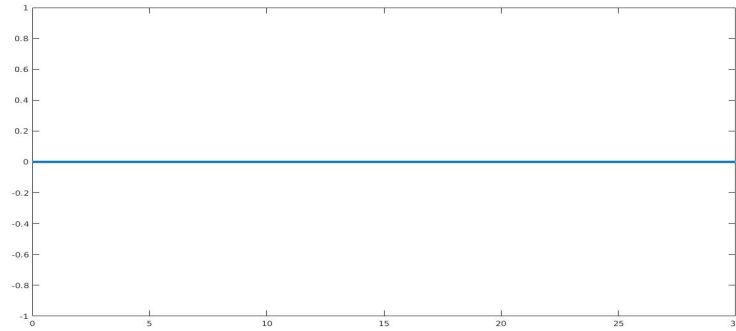


Figure 40: $\text{exponent}(\alpha)$ of Ω_1

Initially the trajectory of Ω_1 does not converge to zero, therefore $\exp(\alpha)$ is decreased to zero, with required accuracy not reached. $\text{Exp}(\alpha)$ becomes 0 increasing the robustness of the system and increaseing the control effort.

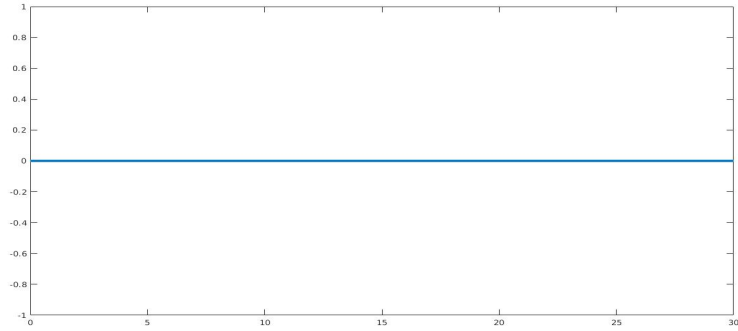


Figure 41: $\text{exponent}(\alpha)$ of Ω_2

8.2 Noisy scenario

A noisy environment has been considered for evaluation. Two scenarios with different sampling time, one with 2 sec and the other with 3 sec. The same white noise is considered and introduced in the wind direction reference. However, the structure orientation is evaluated for change in wind direction for every 10 sec. There is no point of interest to evaluate structure orientation with noisy wind signal for sampling period greater than 10 sec. So its evaluated for 2 and 3 sec. 2 sec not being to realistic. The structure orientation performs well for noisy signal.

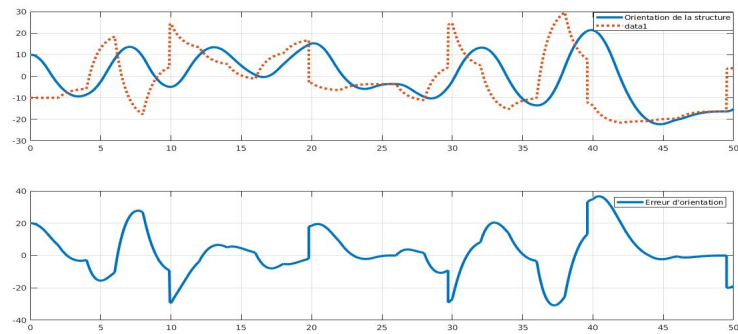


Figure 42: Sampling period 2 sec

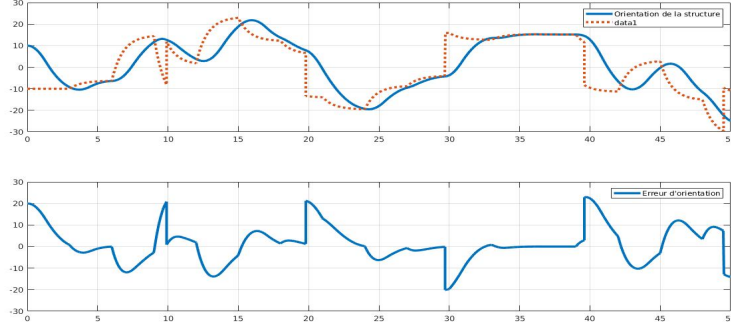
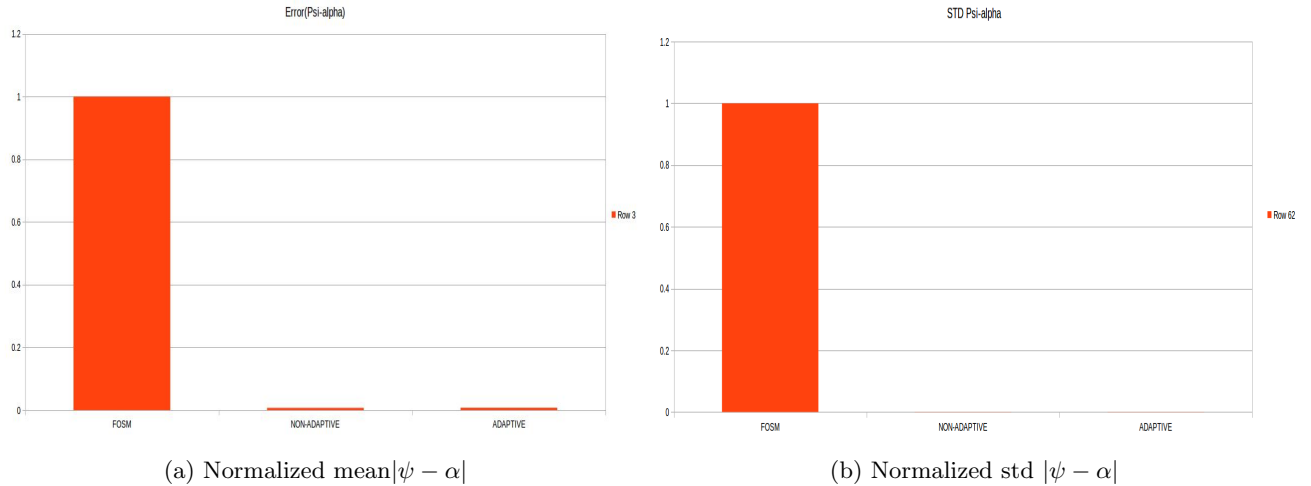
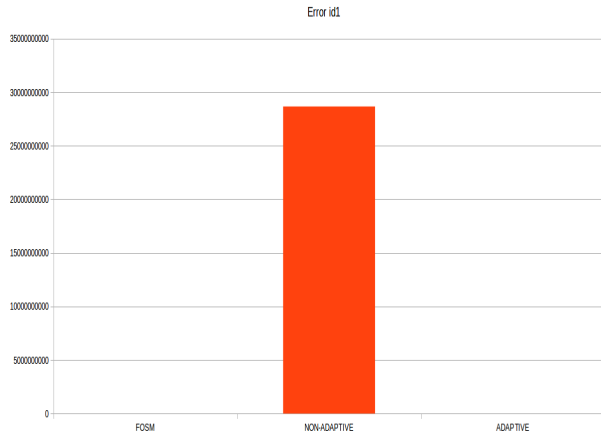


Figure 43: Sampling period 3 sec

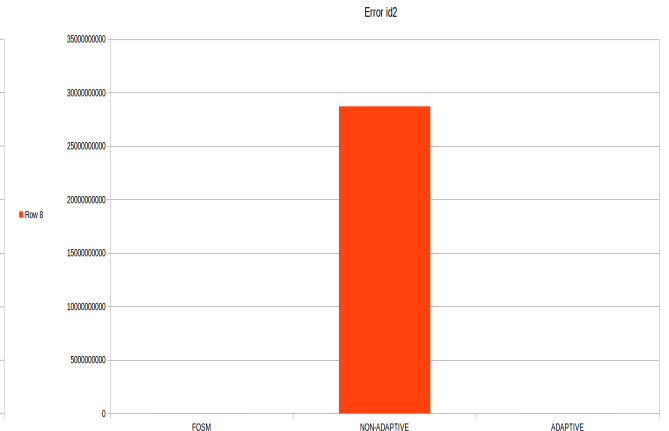
8.2.1 FOSMC vs HOSMC(adaptive and non-adaptive)

A comparison is made between FOSMC and HOSMC. In HOSMC at first attempt we chose to work with non-adaptive, considering all exponents to 0 (twisting controller). In this way, comparison is made between Adaptive and non-adaptive controller. Below figures, represents the normalized value of mean power, structure orientation, currents, Ω tracking and Γ_{em} and its standard deviations (std).

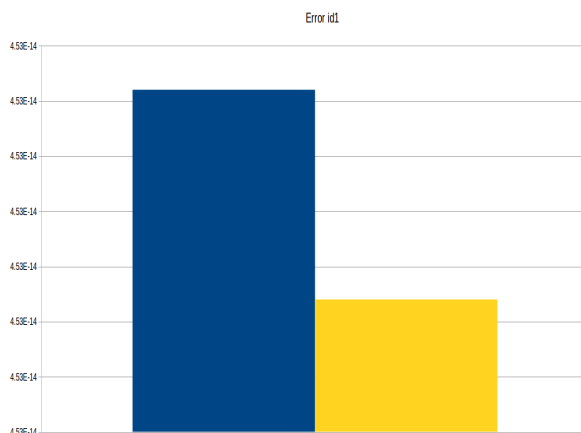




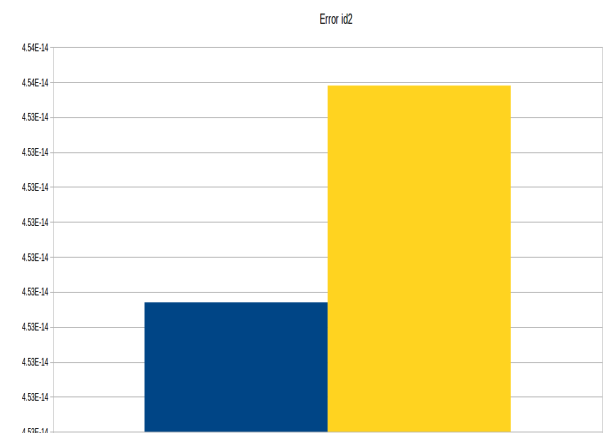
(a) Normalized mean $|i_{d,1}|$



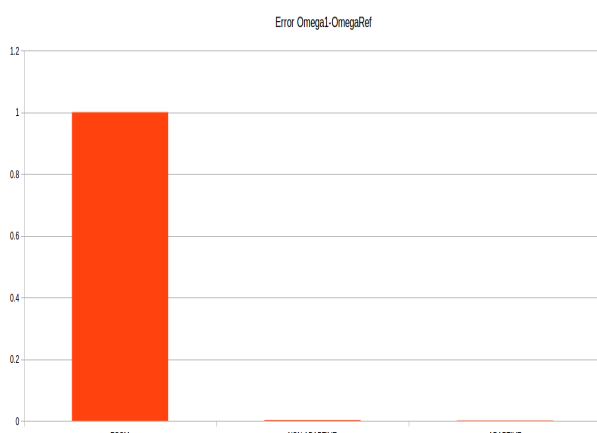
(b) Normalized mean $|i_{d,2}|$



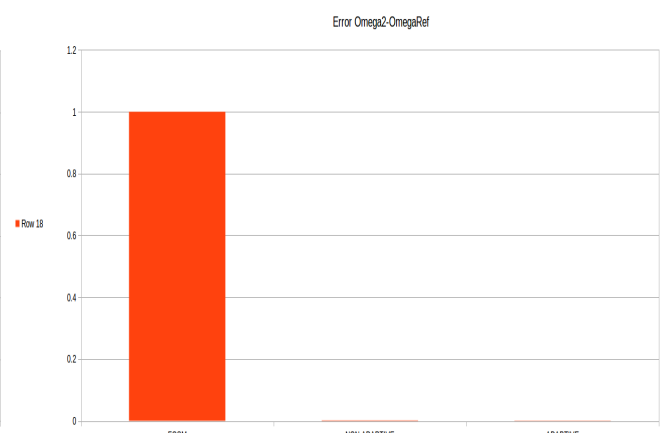
(a) FOSMC vs Adaptive HOSMC



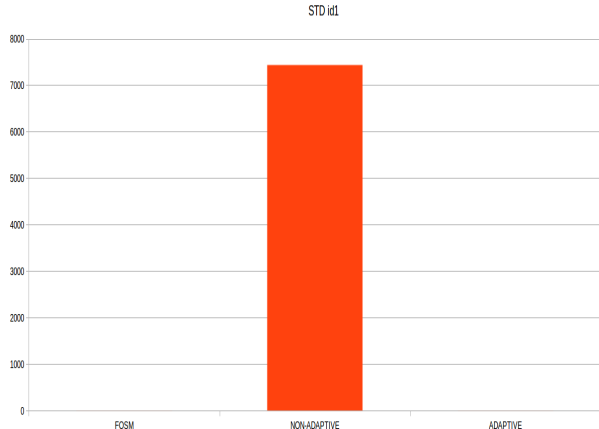
(b) FOSMC vs Adaptive HOSMC



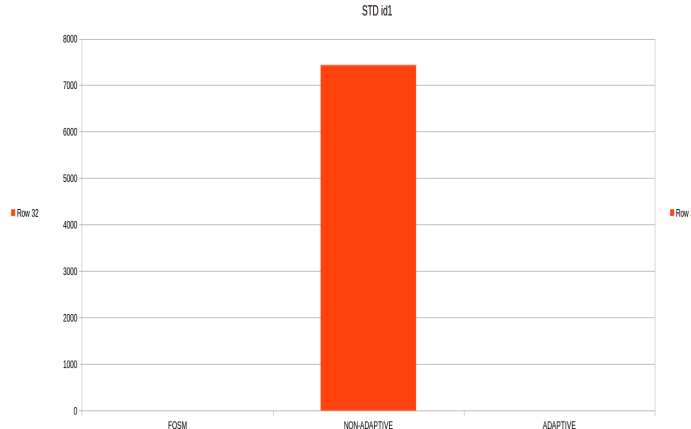
(a) Normalized mean $|\Omega_1 - \Omega_{ref}|$



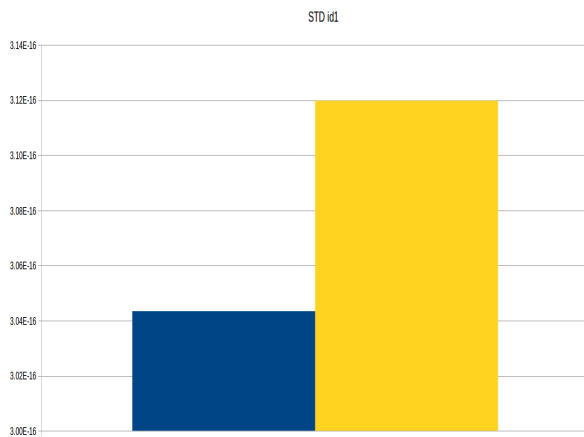
(b) Normalized mean $|\Omega_2 - \Omega_{ref}|$



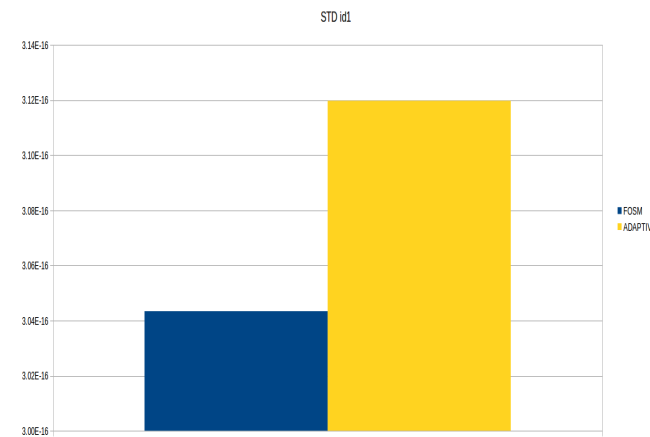
(a) Normalized std $i_{d,1}$



(b) Normalized std $i_{d,2}$

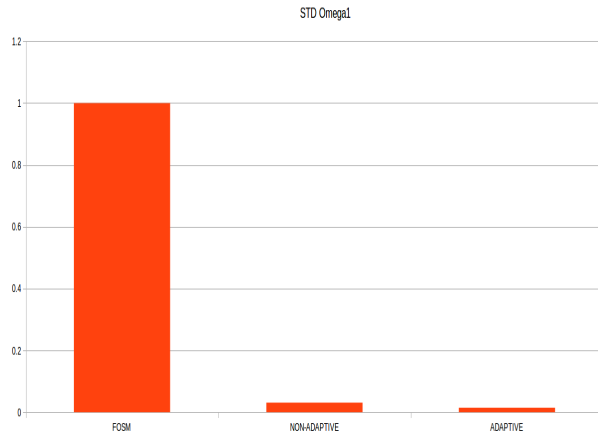


(a) FOSMC vs Adaptive HOSMC

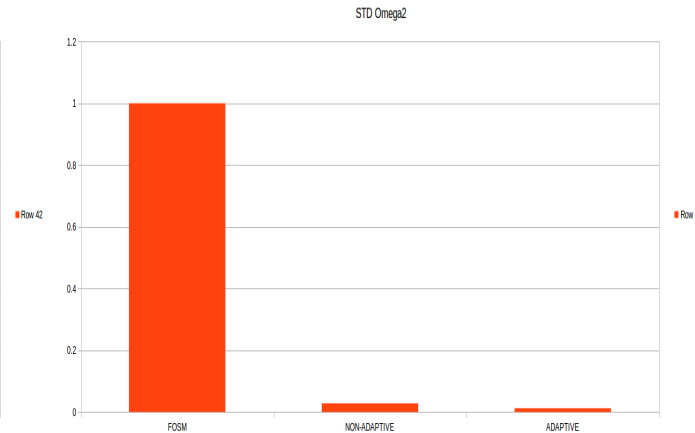


(b) FOSMC vs Adaptive HOSMC

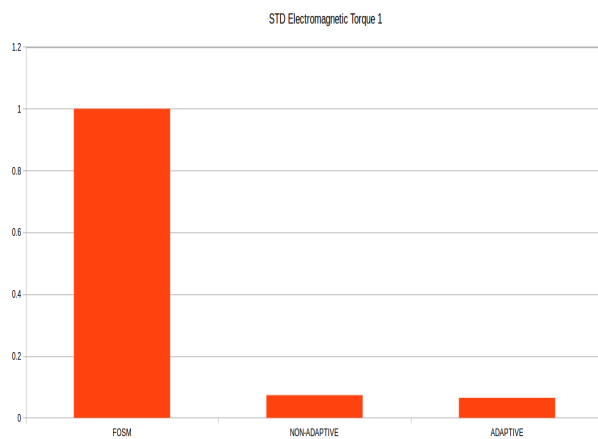
It is a proof that in all the cases adaptive HOSMC is more efficient than non-adaptive HOSMC and FOSMC. For example in case of standard deviations of currents, it appears from the Figure that either FOSMC or Adaptive HOSMC is better among all, but when we compare FOSMC vs Adaptive HOSMC, it appears that FOSMC is better, but what is the difference in the value. It is very very small (10^{-16}), it is negligible.



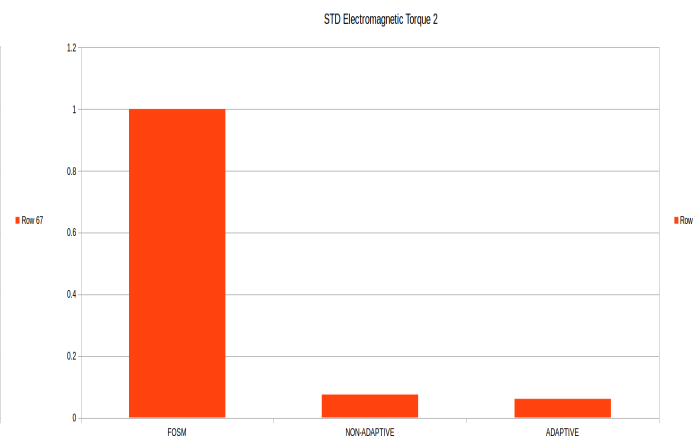
(a) Normalized std Ω_1



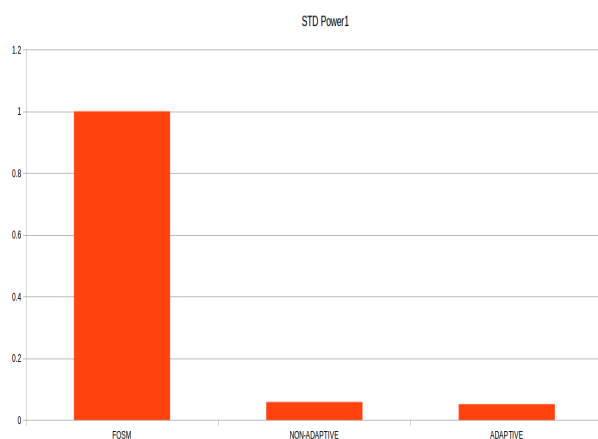
(b) Normalized std Ω_2



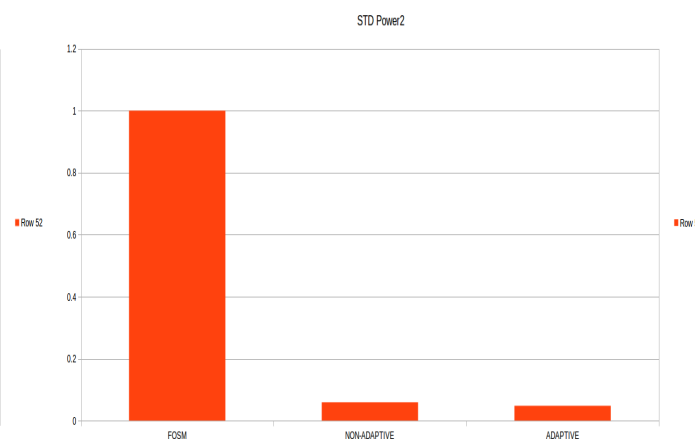
(a) Normalized std $\Gamma_{em,1}$



(b) Normalized std $\Gamma_{em,2}$



(a) Normalized std Power1



(b) Normalized std Power2

9 Wind direction

- The wind direction considered here is not realistic, considering changing the wind direction. Note that the derivative of V is estimated by $\frac{s}{\tau s + 1}$. This is a low-pass filter, so any cut off frequency below 0.01, behaves similarly. For the frequency 0.05 tracking remains almost similar, choosing cut-off frequency greater than 0.05, tracking accuracy decreases. Simulations have been done on Adaptive FOSMC with $\frac{s}{\tau s + 1}$ for estimation of signal derivatives $(\dot{\Omega}, \dot{\Gamma}, \dot{\psi})$.

The time constant τ is chosen as 1/0.01 for the first attempt and using du/dt derivative in the second attempt. The system response behaves like a non-minimum phase system, because the default value of cut-off frequency is 0.

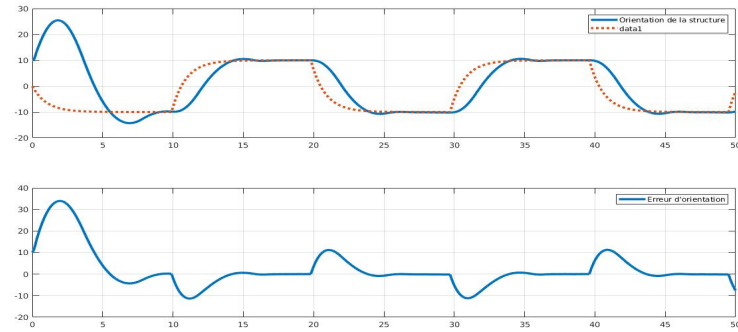


Figure 53: $\psi - \alpha$ tracking with 1st order Filter in-loop and $\tau=1/0.01$

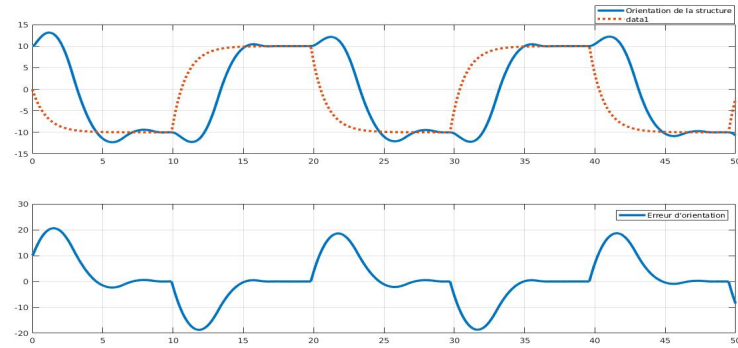


Figure 54: $\psi - \alpha$ tracking with 1st order Filter in-loop using du/dt

with change in wind direction reference, the simulations have been performed on adaptive HOSMC with differentiator [9] for estimation of signal derivatives $(\dot{\Omega}, \dot{\Gamma}, \dot{\psi})$ and the results obtained for structure orientation are:

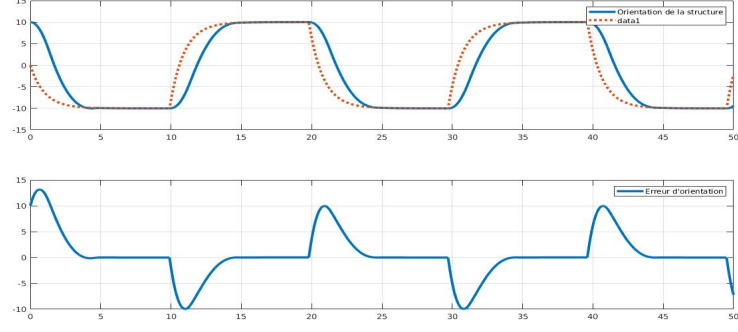


Figure 55: $\psi - \alpha$ tracking with new wind direction

10 Future works

The same procedure is applied for HOSMC of Currents($i_{d,1}, i_{d,2}$) along with HOSMC of Ω . The relative degree of the system is now given as $[3 \ 3 \ 2 \ 3 \ 2]^T$, one defines the sliding vector as

$$\begin{aligned} S_{\psi-\alpha} &= \ddot{\sigma}_{\psi-\alpha}^3 \text{sign}(\ddot{\sigma}_{\psi-\alpha}) + K_{12}^3 [\dot{\sigma}_{\psi-\alpha}^{1.5} \text{sign}(\dot{\sigma}_{\psi-\alpha}) + K_{11}^{1.5}(\sigma_{\psi-\alpha})] \\ S_{\Omega_1-\Omega_1^*} &= \ddot{\sigma}_{\Omega_1-\Omega_1^*}^3 \text{sign}(\ddot{\sigma}_{\Omega_1-\Omega_1^*}) + K_{22}^3 [\dot{\sigma}_{\Omega_1-\Omega_1^*}^{1.5} \text{sign}(\dot{\sigma}_{\Omega_1-\Omega_1^*}) + K_{21}^{1.5}(\sigma_{\Omega_1-\Omega_1^*})] \\ S_{id1} &= \dot{\sigma}_{i_{d,1}}^2 \text{sign}(\dot{\sigma}_{i_{d,1}}) + K_{31}^2(\sigma_{i_{d,1}}) \\ S_{\Omega_2-\Omega_2^*} &= \ddot{\sigma}_{\Omega_2-\Omega_2^*}^3 \text{sign}(\ddot{\sigma}_{\Omega_2-\Omega_2^*}) + K_{42}^3 [\dot{\sigma}_{\Omega_2-\Omega_2^*}^{1.5} \text{sign}(\dot{\sigma}_{\Omega_2-\Omega_2^*}) + K_{41}^{1.5}(\sigma_{\Omega_2-\Omega_2^*})] \\ S_{id2} &= \dot{\sigma}_{i_{d,2}}^2 \text{sign}(\dot{\sigma}_{i_{d,2}}) + K_{51}^2(\sigma_{i_{d,2}}) \end{aligned}$$

With the function $\bar{\varphi}_1(\cdot)$ and $\bar{\varphi}_2(\cdot)$ defined in the sequel,

$$\begin{aligned}
& \left[\left(\lambda_{1\psi} - \frac{D_r}{K_r} \right) \ddot{\psi} - \lambda_{1\psi} \dot{\psi}^* + \lambda_{2\psi} \left(\dot{\psi} - \dot{\psi}^* \right) + \frac{CL}{K_r T_\beta} B (\beta_1 - \beta_2) + \frac{CL}{K_r} (\beta_1 - \beta_2) \dot{B} + \frac{BL}{K_r} (\beta_1 - \beta_2) \dot{C} \right] \\
& \quad \left[\begin{aligned}
& \frac{\dot{\Gamma}_{a1}}{J} + i_{d1} i_{q1} (-2f_2 f_3 f_6 - f_3^2 f_2 - f_1 f_5 f_2 - f_2 f_6^2 - f_1^2 f_4 - \frac{f_1 f_5 f_2}{J} - \frac{f_3 f_2 f_v}{J} \\
& \quad - \frac{f_v f_2 f_6}{J} - \frac{f_2 f_v^2}{J^2}) + \Omega_1 i_{d1}^2 (-3f_2 f_4 f_6 - f_2 f_3 f_4 - \frac{2f_2 f_4 f_v}{J}) - \frac{\dot{\Gamma}_{a1} f_v}{J^2} \\
& \quad + \Omega_1 i_{d1} (-2f_2 f_5 f_6 - f_2 f_3 f_5 - f_1 f_3 f_4 - f_4 f_6 f_1 - \frac{2f_1 f_4 f_v}{J} - \frac{2f_2 f_5 f_v}{J}) + V_{q1} i_{d1} (\frac{2f_2 f_6}{L_q} + \frac{f_2 f_3}{L_q} \\
& \quad + \frac{f_v f_2}{J L_q}) + \Omega_1 i_{q1}^2 (3f_2 f_3 f_7 + f_2 f_6 f_7 + \frac{2f_2 f_7 f_v}{J}) + \Omega_1^2 i_{q1} i_{d1} (4f_2 f_4 f_7) + \Omega_1^2 i_{q1} (3f_2 f_5 f_7 \\
& \quad + f_1 f_4 f_7) + \Omega_1 i_{q1} V_{q1} (-\frac{3f_2 f_7}{L_q}) + V_{d1} i_{q1} (\frac{2f_2 f_3}{L_d} + \frac{f_2 f_v}{J L_d} + \frac{f_2 f_6}{L_d}) + V_{d1} i_{d1} \Omega_1 (\frac{3f_2 f_4}{L_d}) \\
& \quad + V_{d1} \Omega_1 (\frac{2f_2 f_5}{L_d} + \frac{f_1 f_4}{L_d}) + V_{d1} V_{q1} (\frac{-2f_2}{L_d L_q}) + i_{d1}^2 \Gamma_{a1} (\frac{f_2 f_4}{J}) + i_{d1}^3 i_{q1} (-f_2^2 f_4) + i_{d1}^2 i_{q1} (-2f_1 f_2 f_4 - f_2^2 f_5) \\
& \quad + \Gamma_{a1} (\frac{f_v^2}{J^3} + \frac{f_1 f_5}{J^3}) + i_{q1} (-f_1 f_3^2 - f_1^2 f_5 - \frac{f_1 f_3 f_v}{J} - \frac{f_v^2 f_1}{J^2}) + \Omega_1 (-\frac{2f_1 f_5 f_v}{J} \\
& \quad - f_1 f_3 f_5 - \frac{f_v^3}{J^3}) + V_{q1} (\frac{f_1 f_3}{L_q} + \frac{f_1 f_v}{J L_q}) + i_{q1}^2 \Gamma_{a1} (-\frac{f_2 f_7}{J}) + i_{q1}^3 i_{d1} (f_7 f_2^2) \\
& \quad + i_{q1}^3 (f_1 f_2 f_7) + i_{d1} \Gamma_{a1} (\frac{f_2 f_5 + f_1 f_4}{J}) - \frac{\lambda_{opt}}{R_s} (\cos(\psi - \alpha) (-3V \dot{\psi}^2 - 3V \dot{\psi} \ddot{\psi}) + \\
& \quad \sin(\psi - \alpha) (-3V \ddot{\psi} - 3V \dot{\psi} + V \dot{\psi}^3 - V \ddot{\psi})) \\
& \quad i_{d1} \frac{R_s^2}{L_d^2} - \Omega_1 i_{q1} \left[\frac{p R_s (L_q - L_d)}{L_d^2} \right] - V_{d1} \frac{R_s}{L_d^2} \\
& \quad - \Omega_1^2 i_{d1} p^2 - \Omega_1^2 p^2 \frac{\phi_f}{L_d} + \Omega_1 V_{q1} \frac{p}{L_d} \\
& \quad \frac{\dot{\Gamma}_{a2}}{J} + i_{d2} i_{q2} (-2f_2 f_3 f_6 - f_3^2 f_2 - f_1 f_5 f_2 - f_2 f_6^2 - f_1^2 f_4 - \frac{f_1 f_5 f_2}{J} - \frac{f_3 f_2 f_v}{J} \\
& \quad - \frac{f_v f_2 f_6}{J} - \frac{f_2 f_v^2}{J^2}) + \Omega_2 i_{d2}^2 (-3f_2 f_4 f_6 - f_2 f_3 f_4 - \frac{2f_2 f_4 f_v}{J}) - \frac{\dot{\Gamma}_{a2} f_v}{J^2} \\
& \quad + \Omega_2 i_{d2} (-2f_2 f_5 f_6 - f_2 f_3 f_5 - f_1 f_3 f_4 - f_4 f_6 f_1 - \frac{2f_1 f_4 f_v}{J} - \frac{2f_2 f_5 f_v}{J}) + V_{q2} i_{d2} (\frac{2f_2 f_6}{L_q} + \frac{f_2 f_3}{L_q} \\
& \quad + \frac{f_v f_2}{J L_q}) + \Omega_2 i_{q2}^2 (3f_2 f_3 f_7 + f_2 f_6 f_7 + \frac{2f_2 f_7 f_v}{J}) + \Omega_2^2 i_{q2} i_{d2} (4f_2 f_4 f_7) + \Omega_2^2 i_{q2} (3f_2 f_5 f_7 \\
& \quad + f_1 f_4 f_7) + \Omega_2 i_{q2} V_{q2} (-\frac{3f_2 f_7}{L_q}) + V_{d2} i_{q2} (\frac{2f_2 f_3}{L_d} + \frac{f_2 f_v}{J L_d} + \frac{f_2 f_6}{L_d}) + V_{d2} i_{d2} \Omega_2 (\frac{3f_2 f_4}{L_d}) \\
& \quad + V_{d2} \Omega_2 (\frac{2f_2 f_5}{L_d} + \frac{f_1 f_4}{L_d}) + V_{d2} V_{q2} (\frac{-2f_2}{L_d L_q}) + i_{d2}^2 \Gamma_{a2} (\frac{f_2 f_4}{J}) + i_{d2}^3 i_{q2} (-f_2^2 f_4) + i_{d2}^2 i_{q2} (-2f_1 f_2 f_4 - f_2^2 f_5) \\
& \quad + \Gamma_{a2} (\frac{f_v^2}{J^3} + \frac{f_1 f_5}{J^3}) + i_{q2} (-f_1 f_3^2 - f_1^2 f_5 - \frac{f_1 f_3 f_v}{J} - \frac{f_v^2 f_1}{J^2}) + \Omega_2 (-\frac{2f_1 f_5 f_v}{J} \\
& \quad - f_1 f_3 f_5 - \frac{f_v^3}{J^3}) + V_{q2} (\frac{f_1 f_3}{L_q} + \frac{f_1 f_v}{J L_q}) + i_{q2}^2 \Gamma_{a2} (-\frac{f_2 f_7}{J}) + i_{q2}^3 i_{d2} (f_7 f_2^2) \\
& \quad + i_{q2}^3 (f_1 f_2 f_7) + i_{d2} \Gamma_{a2} (\frac{f_2 f_5 + f_1 f_4}{J}) - \frac{\lambda_{opt}}{R_s} (\cos(\psi - \alpha) (-3V \dot{\psi}^2 - 3V \dot{\psi} \ddot{\psi}) + \\
& \quad \sin(\psi - \alpha) (-3V \ddot{\psi} - 3V \dot{\psi} + V \dot{\psi}^3 - V \ddot{\psi})) \\
& \quad i_{d2} \frac{R_s^2}{L_d^2} - \Omega_2 i_{q2} \left[\frac{p R_s (L_q - L_d)}{L_d^2} \right] - V_{d2} \frac{R_s}{L_d^2} \\
& \quad - \Omega_2^2 i_{d2} p^2 - \Omega_2^2 p^2 \frac{\phi_f}{L_d} + \Omega_2 V_{q2} \frac{p}{L_d}
\end{aligned} \right] \tag{41}$$

$$\bar{\varphi}_2(\cdot) = \begin{bmatrix} \frac{-2}{K_r T_\beta} LCB & 0 & 0 & 0 & 0 \\ 0 & \frac{-f_2}{L_d} i_{q1} & \frac{-1}{L_q} (f_1 + f_2 i_{d1}) & 0 & 0 \\ 0 & \frac{1}{L_d} & 0 & 0 & 0 \\ 0 & 0 & 0 & \frac{-f_2}{L_d} i_{q2} & \frac{-1}{L_q} (f_1 + f_2 i_{d2}) \\ 0 & 0 & 0 & \frac{1}{L_d} & 0 \end{bmatrix} \tag{42}$$

The control input is defined as,

$$\begin{bmatrix} \Delta\beta \\ V_{d_1} \\ V_{q_1} \\ V_{d_2} \\ V_{q_2} \end{bmatrix} = [\varphi_2(\cdot)]^{-1}[-\varphi_1(\cdot) + \begin{bmatrix} -K_{13}S_{\psi-\alpha} \exp^1 sign(S_{\psi-\alpha}) \\ -\int K_{23}S_{\Omega_1-\Omega_1^*} \exp^2 sign(S_{\Omega_1-\Omega_1^*}) \\ -\int K_{32}S_{id1} \exp^3 sign(S_{id1}) \\ -\int K_{43}S_{\Omega_2-\Omega_2^*} \exp^4 sign(S_{\Omega_2-\Omega_2^*}) \\ -\int K_{52}S_{id2} \exp^5 sign(S_{id2}) \end{bmatrix}] \quad (43)$$

10.1 Results

The obtained results for HOSMC of i_d and Ω are presented in here,

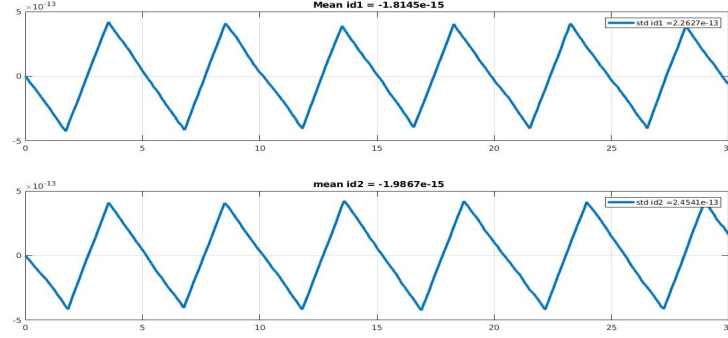


Figure 56: Currents with Differentiator in-loop

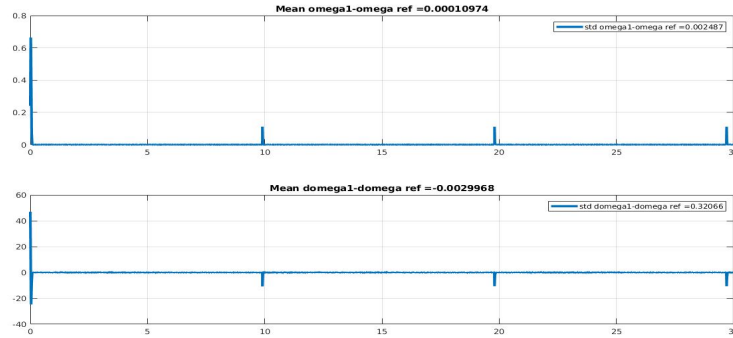


Figure 57: Ω_1 tracking with Differentiator in-loop

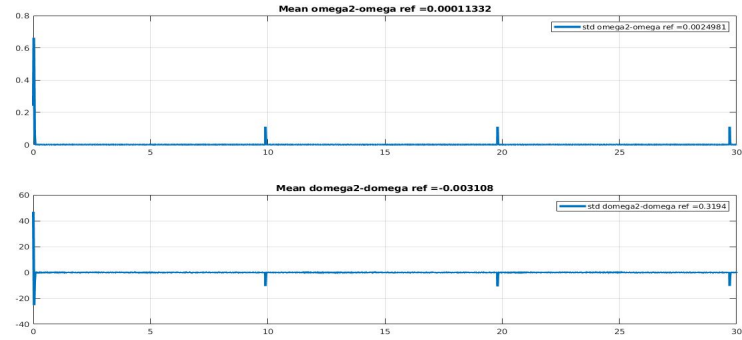


Figure 58: Ω_2 tracking with Differentiator in-loop

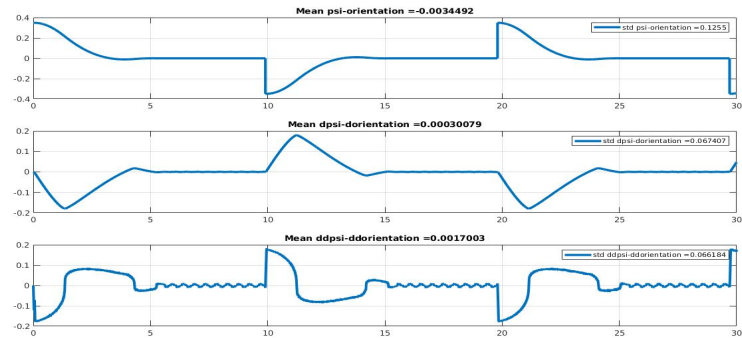


Figure 59: $\psi - \alpha$ and its derivatives with Differentiator in-loop

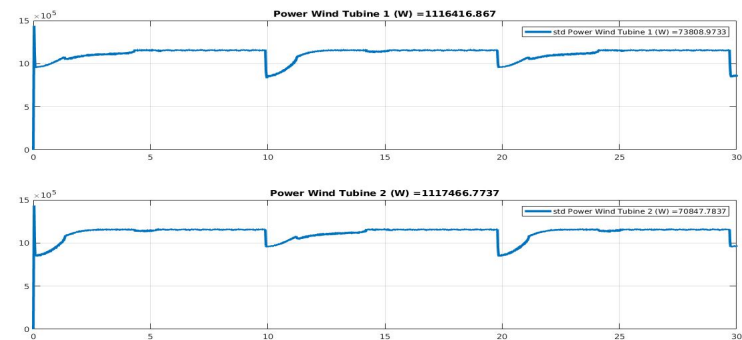


Figure 60: Power with Differentiator in-loop

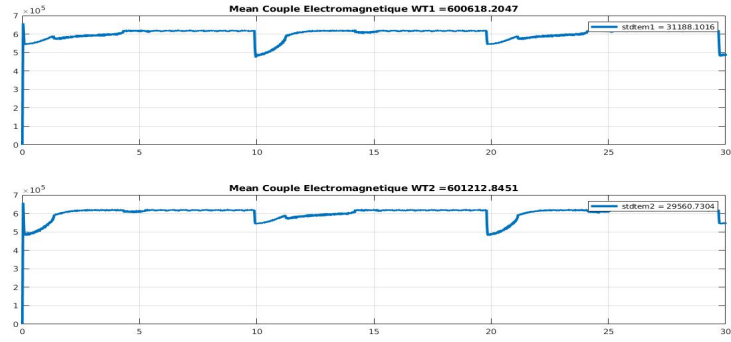


Figure 61: Γ tracking with Differentiator in-loop

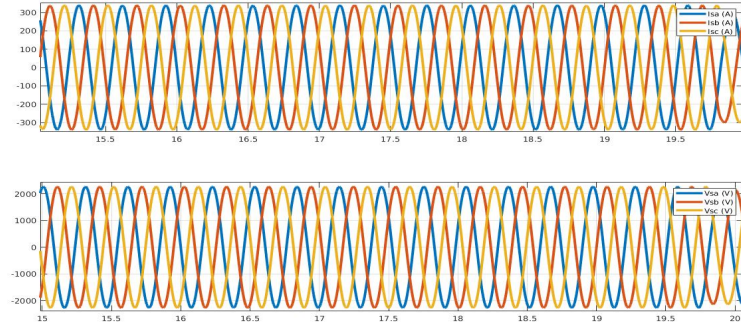


Figure 62: 3 phase voltage and currents with Differentiator in-loop

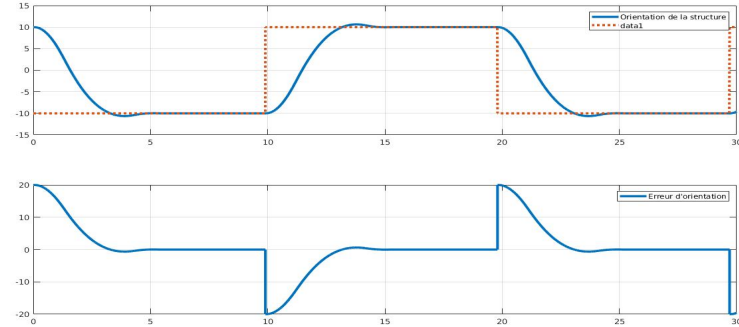


Figure 63: $\psi - \alpha$ tracking with Differentiator in-loop

Table 8: Comparision of Ω HOSMC with Ω and i_d HOSMC

Parameters	Ω	Ω, i_d
$i_{d,1}$	$-4.5322e^{-14}$	$-1.8145e^{-15}$
std $i_{d,1}$	$3.1198e^{-16}$	$2.2627e^{-13}$
$i_{d,2}$	$-4.5349e^{-14}$	$-1.9867e^{-15}$
std $i_{d,2}$	$3.2459e^{-16}$	$2.4541e^{-13}$
Ω_2	$5.8313e^{-6}$	0.00011332
std Ω_2	0.000147	0.0024981
Ω_1	$9.8229e^{-6}$	0.00010974
std Ω_1	0.00015962	0.002487
$\psi - \alpha$	$-1.6466e^{-5}$	-0.0034492
Power1	1155219.4657	1116416.867
std Power1	3984.957	73808.9733
Power2	1155267.0806	1117466.7737
std Power2	3538.5249	70847.7837
$\Gamma_{em,1}$	617168.824	600618.2047
std $\Gamma_{em,1}$	2133.4456	31188.1016
$\Gamma_{em,2}$	617195.5757	601212.8451
std $\Gamma_{em,2}$	1894.8731	29560.7304

- From the above table we can see that the results obtained for Ω and i_d HOSMC is not efficient as just Ω HOSMC.
- The differentiator estimates the signal well for Γ , but not so perfect for \dot{V} . The reasons could be bad tuning. Some different approach might be necessary.

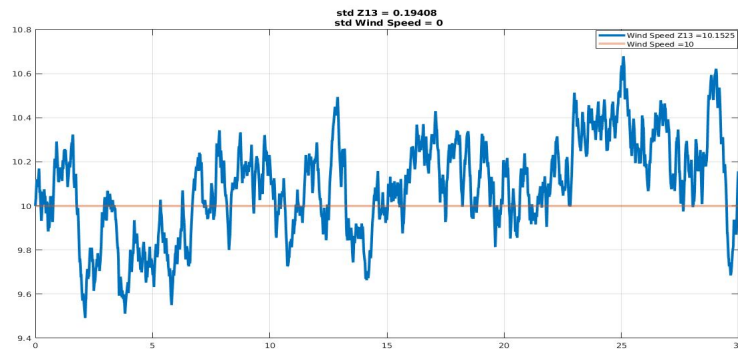


Figure 64: Wind speed(V) Original signal vs Differentiator(in-loop)

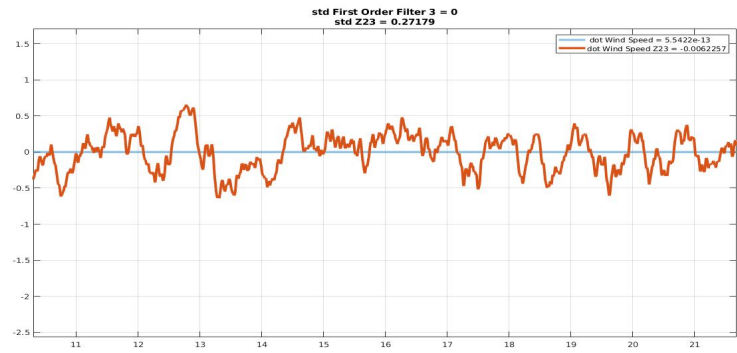


Figure 65: Wind speed(\dot{V}) Filter vs Differentiator(in-loop)(zoom)

11 Conclusion

A new control methodology based on HOSMC ensures high accuracy tracking and requires low control effort with reduced chattering/oscillations. This is done by varying a parameter α on the exponent term of the controller. This control law ensures power output maximization, with reduced electromagnetic torque oscillations resulting in the improvement of the structure lifetime. Simulations were performed in different scenarios(Perturbation/uncertainties). Though pitch angle oscillations have not been discussed here, pitch angle oscillations are also reduced. Future work have been presented in the report.

References

- [1] A. Herskovits, O. Laffitte, P. Thome, and A. Tobie, "V-shaped, bi-rotor wind generator on a spar floating structure," French Patent WO2014060420 A1, 2014.
- [2] Corradini, M. L., Ippoliti, G., Orlando, G. (2013). Robust control of variable-speed wind turbines based on an aerodynamic torque observer. *IEEE Transactions on Control Systems Technology*, 21(4), 1199-1206.
- [3] Huang, C., Li, F., Ding, T., Jin, Z., Ma, X.(2015a). Second-order cone programming based optimal control strategy for wind energy conversion systems over complete operating regions. *IEEE Transactions on Sustainable Energy*, 6(1), 263-271.
- [4] Saravananumar, R., Jena, D.(2015). Validation of an integral sliding mode control for optimal control of a three blade variable speed variable pitch wind turbines. *Electrical Power and Energy Systems*, 69, 421-429.
- [5] I. Guenoune, F. Plestan, A. Chermitti, and C. Evangelista,"Modeling and robust control of a twin wind turbines structure,"*Control Engineering Practice*, vol. 69, pp. 23 – 25, 2017.
- [6] A. Mesemanolis and C. Mademlis, "Combined maximum power point and yaw control strategy for a horizontal axis wind turbine," in *International Conference on Electrical Machines*, Berlin, Germany, 2014 .
- [7] I. Guenoune, F. Plestan, and A. Chermitti,"Yaw rotation control of a twin wind turbines structure: super-twisting strategy," in *IEEE Conference on Control Technology and Applications*, Kohala Coast, Hawaii, USA, 2017.
- [8] A. Levant, "Sliding order and sliding accuracy in sliding mode control," *International Journal of Control*, vol. 58 – 6, pp. 1247– 1463, 1993.
- [9] M. Ghanes, J.P. Barbot, L. Fridman, and A. Levant, "A novel differentiator: a compromise between super-twisting and linear algorithms," in *IEEE conf. on Decision and Control*, Melbourne, Australia, 2017.
- [10] M. Ghanes, J.P. Barbot, L. Fridman, and A. Levant, "A second order sliding mode differentiator with a variable exponent" in *American Control Conference*, Sheraton Seattle Hotel, Seattle, USA, May 24 – 26, 2017.
- [11] V.I Utkin, *Sliding modes in control and optimization*. Springer-Verlag Berlin Heidelberg, 1992.
- [12] Y.Shtessel, C.Edwards, L.Fridman, and A.Levant, *Sliding mode control and observation*. Springer,2014.
- [13] I. Munteanu, A. Bratu, N. Cutululis, and C. Emil, *Optimal Control of Wind Energy Systems*. Advances in Industrial Control, Springer, 2008 .
- [14] Uehara, A., Pratap, A., Goya, T., senjuu, T., Yona, A., Urasaki, N., et al.(2011). A coordinated control method to smooth wind power fluctuations of pmsg-based wecs. *IEEE Transactions on Energy Conversion*,26(2),550-558
- [15] Beltran, B., Ahmed-Ali, T., Benbouzid, M. (2008). Sliding mode power control of variable-speed wind energy conversion systems. *IEEE Transactions on Energy conversion*,23(2),551-558.
- [16] Eberhart, P., Chung, T. S., Haumer, A., Kral, C. (2015). Open source library for the simulation of wind power plants. In *International Modelica Conference*. Versaille, France.
- [17] Tan, L. V., Thanh, H. N., Dong, C. L. (2015). Advanced pitch angle control based on fuzzy logic for variable-speed wind turbine systems. *IEEE Transactions on Energy Conversion*, 30(2), 578–587.
- [18] Georg, S., Schulte, H., Aschemann, H. (2012). Control-oriented modelling of wind turbines using a Takagi-Sugeno model structure. In *IEEE International Conference on Fuzzy Systems*. Brisbane, Australia.
- [19] Huang, C., Li, F., Jin, Z. (2015b). Maximum power point tracking strategy for large-scale wind turbine dynamics. *IEEE Transactions on Industrial Electronics*, 62(4), 2530–2539.

- [20] Hamida, M., de Leon Morales, J., Glumineau, A., Boisliveau, R. (2013). An adaptive interconnected observer for sensorless control of PM synchronous motors with online parameter identification. *IEEE Transactions on Industrial Electronics*, 60(2), 739.
- [21] Glumineau, A., de Leon-Morales, J. (2015). Sensorless AC electric motor control robust advanced design techniques and applications. Berlin, Germany: Springer.
- [22] Munteanu, I., Bratcu, A., Cutululis, N., Emil, C. (2008). Advances in industrial control. Optimal control of wind energy systems. Berlin, Germany: Springer.
- [23] Shariatpanah, H., Fadaeinedjad, R., Rashidinejad, M. (2013). A new model for pmsg- based wind turbine with yaw control. *IEEE Transactions on Energy Conversion*, 28(4), 929–937.
- [24] Ezzat, M., Glumineau, A., Plestan, F. Sensorless high order sliding mode control of permanent magnet synchronous motor. In International workshop on variable structure systems. Mexico City, Mexico, 2010.
- [25] Hamida, M., Glumineau, A., De Leon, J. (2012). Robust integral backstepping control for sensorless IPM synchronous motor controller. *Journal of the Franklin Institute*, 349(5), 1734–1757.
- [26] Aghatehrani, R., Kavasseri, R. (2013). Sensitivity-analysis-based sliding mode control for voltage regulation in microgrids. *IEEE Transactions on Sustainable Energy*, 4(1), 50–57.
- [27] Traore, D., Plestan, F., Glumineau, A., de Leon, J. (2008). Sensorless induction motor: High-order sliding-mode controller and adaptive interconnected observer. *IEEE Transactions on Industrial Electronics*, 55(11), 3818–3827.
- [28] Utkin, V., Guldner, J., Shi, J. (1999). Sliding mode control in electro-mechanical Systems. New York, USA: Taylor Francis.
- [29] Isidori, A. (1999). Nonlinear control systems. London, UK: Springer.
- [30] E. Tahoumi, M. Ghanes, F. Plestan, and J.-P. Barbot, “A new controller switching between linear and twisting algorithms,” in 2018 Annual American Control Conference (ACC), pp. 6150–6155, IEEE, 2018.
- [31] E. Tahoumi, F. Plestan, M. Ghanes, and J.-P. Barbot, “Adaptive exponent parameter: a robust control solution balancing between linear and twisting controllers,” in 2018 15th International Workshop on Variable Structure Systems (VSS), pp. 186–191, IEEE, 2018.
- [32] E. Tahoumi, F. Plestan, M. Ghanes, and J.-P. Barbot, “A controller switching between twisting and linear algorithms for an electropneumatic actuator,” in 2018 European Control Conference (ECC), pp. 2368–2373, IEEE, 2018.
- [33] E. Tahoumi, F. Plestan, M. Ghanes, and J.P. Barbot, ”Robust and energy efficient control schemes based on higher order sliding mode,” in 2019 European Control Conference(ECC).
- [34] E. Tahoumi, C.Evangelista, F. Plestan, M. Ghanes, J.P. Barbot, P.Puleston, ”Energy efficient control with adaptive parameters derived from homogeneous algorithms-Application to a wind system,” in 2019 Control Engineering Practice.
- [35] Corradini, M. L., Ippoliti, G., Orlando, G. (2013). Robust control of variable-speed wind turbines based on an aerodynamic torque observer. *IEEE Transactions on Control Systems Technology*, 21(4), 1199–1206.
- [36] F. Plestan, E. Moulay, A. Glumineau, and T. Cheviron, ”Robust output feedback sampling control based on second order sliding mode, ” Automatica, vol.46, no. 6, pp.1096-1100, 2010.
- [37] X. Yan, A. Estrada., and F.Plestan, ”Adaptive pulse output feedback controller based on second-order sliding mode: Methodology and application,” *IEEE Transactions on Control Systems Technology*, vol.24, no. 6, pp. 2233-2240, 2016.

- [38] F. Plestan, E. Moulay and A. Glumineau, " Output feedback sampling control: a robust solution based on second order sliding mode control, "IEEE Conference on Decision and Control and 28th Chinese Control Conference Shanghai, P.R. China, December 16-18, 2009.
- [39] Yan, J., Lin, H., Feng, Y., Guo, X., Huang, Y., Zhu, Z. (2012). Improved sliding mode model reference adaptive system speed observer for fuzzy control of direct-drive permanent magnet synchronous generator wind power generation system. *IET Renewable Power Generation*, 7 (1), 28–35.
- [40] Jafarnejadsani, H., Pieper, J., Ehlers, J. (2013). Adaptive control of a variable-speed variable-pitch wind turbine using radial-basis function neural network. *IEEE Transactions on Control Systems Technology*, 21(6), 2264–2272.
- [41] L.fridman, F. Plestan and J.P. Barbot, Recent trends in sliding mode control. 2015.
- [42] C.Edwards and S.Spurgeon, Sliding mode control: theory and applications. Crc Press, 1998.
- [43] A. Levant. "Homogeneity approach to high-order sliding mode design." *Automatica* 41.5 (2005): 823-830.
- [44] A. Polyakov and A. Poznyak. Lyapunov function design for finite-time convergence analysis: "twisting" controller for second order sliding mode realization. *Automatica*, 45.2 (2009): 444-448.
- [45] A. Polyakov and A. Poznyak. Unified Lyapunov function for a finite-time stability analysis of relay second-order sliding mode control systems. *IMA journal of Mathematical Control and Information*, 29.4 (2012) 529-550.
- [46] Tang, C. Y., Guo, Y., Jiang, J. N. (2011). Nonlinear dual-mode control of variable-speed wind turbines with doubly fed induction generators. *IEEE Transactions on Control Systems Technology*, 19(4), 744–756.
- [47] Corradini, M. L., Ippoliti, G., Orlando, G. (2013). Robust control of variable-speed wind turbines based on an aerodynamic torque observer. *IEEE Transactions on Control Systems Technology*, 21(4), 1199–1206.